NACA RM A54A29

NACA

RESEARCH MEMORANDUM

AN EXPERIMENTAL INVESTIGATION OF THE FLUTTER OF SEVERAL WINGS OF VARYING ASPECT RATIO, DENSITY, AND THICKNESS RATIO AT MACH NUMBERS FROM 0.60 TO 1.10

By Raymond Herrera and Robert H. Barnes

Ames Aeronautical Laboratory
Moffett Field, Calif.

NATIONAL ADVISORY COMMITTEE
FOR AERONAUTICS

WASHINGTON

April 7, 1954

NACA RM A54A29

NATIONAL ADVISORY COMMITTEE FOR AERONAUTICS

RESEARCH MEMORANDUM

AN EXPERIMENTAL INVESTIGATION OF THE FLUTTER OF SEVERAL WINGS OF VARYING ASPECT RATIO, DENSITY, AND THICKNESS RATIO AT MACH NUMBERS FROM 0.60 TO 1.10

By Raymond Herrera and Robert H. Barnes

SUMMARY

An experimental investigation has been conducted to determine the flutter characteristics of several rectangular wings of variable aspect ratio at Mach numbers from 0.60 to 1.10. The wings were solid aluminum or steel and were 2, 4, and 6 percent thick.

Flutter was encountered at both low and high angles of attack. At low angles of attack, the flutter frequencies were of the order of the first natural bending frequencies even though the modes were of the bending-torsion type. At high angles of attack, the modes were essentially pure torsion and the frequencies were nearly equal to the first natural torsion frequencies. In most cases where stall flutter occurred, it occurred below maximum static lift.

INTRODUCTION

Flutter may be classified according to the nature of the unsteady flow by which it is sustained. Accordingly, that class of flutter accompanied by attached or potential flow has been termed classical flutter. It may occur in subsonic, transonic, or supersonic flow and may involve either single or multiple degrees of freedom. However, according to potential theory, classical flutter is not dependent upon angle of attack. A second type of flutter is associated with separated flow and is related to angle of attack. If flutter occurs at high angles of attack it is often termed stall flutter. However, a separation-type flutter may occur at low or moderate angles of attack at transonic speeds and it is not always possible to establish a definite boundary between this type of flutter and classical flutter.

The status of research on classical flutter indicates that there is a need for experimental research at transonic speeds. Separation-type flutter at high subsonic and transonic Mach numbers has become of interest because of its occurrence on missiles (ref. 1) and because of the need for data which are applicable to the design of high-speed aircraft having thin wings (ref. 2). The present investigation was undertaken to provide such experimental flutter data for a series of rectangular wings of varying aspect ratio. The tests were performed on the transonic bump of the Ames 16-foot high-speed wind tunnel at Mach numbers ranging from 0.60 to 1.10, corresponding to a Reynolds number range from 1.7 to 2.0 million.

SYMBOLS

A	aspect ratio, full span
EI	bending stiffness, lb-in.^{2}
GJ	torsional stiffness, lb-in.^{2}
I_α	polar moment of inertia about the elastic axis per unit length, slug-ft^2/ft
M	Mach number
V	velocity, ft/sec
$\frac{V}{b\omega_\alpha}$	reduced velocity
b	wing semichord
g	damping coefficient
g_α	structural damping coefficient for the torsion mode
g_h	structural damping coefficient for the bending mode
m	mass per unit length, slugs/ft
r_α	dimensionless radius of gyration of wing section, $\sqrt{I_\alpha/mb^2}$
$x_{c.g.}$	center of gravity location from leading edge, percent chord
$x_{e.a.}$	elastic axis location from leading edge, percent chord
α	angle of attack, deg

α_f minimum angle of attack at which stall flutter occurred, deg

μ mass density ratio, $\frac{m}{\pi\rho_0 b^2}$

ρ tunnel air density, slugs/cu ft

ρ_0 air density at sea level, slugs/cu ft

ω_α first natural torsional frequency, radians/sec

ω_h first natural bending frequency, radians/sec

MODELS

The seven rectangular wings tested had symmetrical NACA 64A-series sections with thickness-to-chord ratios of 0.02, 0.04, or 0.06. The models had 0.5-foot chords and were constructed of solid steel or aluminum. Two of the aluminum wings, 4 percent and 6 percent thick, were modified by cutting spanwise slots 0.005 inch wide in the upper and lower surfaces to reduce the torsional stiffness. The models are designated in this report by a number which indicates the thickness (2, 4, or 6 percent) followed by a letter to signify the material (A or S). A letter X is used to designate a slotted wing. Thus, wing 4AX indicates a 64A004 aluminum wing with spanwise slots.

The following physical characteristics are given for each wing in table I: mass density ratio, radius of gyration, bending stiffness, torsional stiffness, elastic axis, and center of gravity. Values of $b\omega_h$ and $b\omega_\alpha$ based on the experimentally determined natural first bending and first torsional frequencies are given in table II for various aspect ratios of each wing. The structural damping coefficients of wings 2S, 4S, 4A, and 4AX which were determined experimentally are presented in table III.

EXPERIMENTAL DETERMINATION OF THE ELASTIC AXES AND NATURAL FREQUENCIES

The elastic axis of each wing was determined by noting the movement of a reflected light beam while a weight near the tip was moved in the chordwise direction. The distance of the weight from the leading edge for which torsional deflection of the wing could not be detected is given in table I for each model in percent chord. The wings were so mounted as to have their maximum aspect ratios for these measurements.

The resonant frequencies were determined in the wind tunnel prior to testing. The equipment used for their determination is shown in the schematic and block diagrams of figure 1. The output of an audio oscillator was amplified and used to drive two 12-inch speakers. The speakers, mounted above and below the model, were used to excite the model through two strings attached to the speaker cones. The output of a crystal vibration pickup mounted at the wing tip and a reference signal from the driving oscillator were used to display Lissajous patterns on an oscilloscope. These patterns permitted the operator to ascertain the resonant frequency.

For the purpose of exciting the bending mode, the speakers were located in line with the elastic axis; for exciting torsion, the speakers were offset to each side of the elastic axis and their polarities were so related that a couple was produced.

EXPERIMENTAL DETERMINATION OF STRUCTURAL DAMPING

The structural damping of wings 2S, 4S, 4A, and 4AX at various aspect ratios was determined by means of a free-oscillation technique. Bending oscillations were excited by the sudden release of a weight suspended from the tip at the elastic axis. A weight of 6.25 pounds was used on all wings except 2S for which a weight of 5 pounds was used. Torsional vibrations were excited by a sharp blow struck on the leading edge near the tip. This procedure unavoidably introduced a small amount of bending which probably influenced the calculated damping coefficients.

The motion of the wing tip was detected by a small crystal accelerometer whose mass was considered to have negligible effect on the results. The output of this accelerometer was recorded on an oscillograph. From these records the logarithmic decrement was determined for intervals of about 20 cycles and the structural damping coefficient was calculated according to the following relationship (see ref. 3):

$$g = \frac{1}{\pi} \text{ (logarithmic decrement)}$$

The coefficients so determined from several records were averaged and the results are presented in table III.

TUNNEL TEST APPARATUS AND INSTRUMENTATION

The tests were conducted on the transonic bump of the Ames 16-foot high-speed wind tunnel. The wings were movable spanwise through clamps contoured to the wing profiles. The models were so positioned as to provide the desired aspect ratio and were then clamped by a force of

800 pounds obtained through the action of an air cylinder. The aspect ratio was varied from 2 to 6 for the 4- and 6-percent-thick wings and from 1 to 4 for the 2-percent-thick wings. The maximum angle of attack was limited to 19.5° by the angle-of-attack mechanism.

The flutter frequencies were determined with the aid of a modified phonograph crystal cartridge mounted between the upper clamping block and the tunnel wall. The wing vibrations were transmitted to the pickup through a short stiff wire resting on the upper surface of the wing. When the vibrations were at a constant frequency, the signal from the pickup was used in conjunction with a reference signal from an audio oscillator to display Lissajous patterns on an oscilloscope.

A high-speed motion-picture camera (1100 frames per second) was mounted outside the test section, opposite and slightly above the model and was used to photograph the upper surface and the wing tip when flutter occurred. The motion-picture records were used to aid in the qualitative determination of the flutter modes.

METHOD OF TESTING

The Mach number range investigated was from 0.60 to 1.10, corresponding to a Reynolds number range from 1.7 to 2.0 million. The variation of velocity and relative density with Mach number is given in figure 2. At each test Mach number selected, the model was set at 0° angle of attack and so clamped as to provide its minimum aspect ratio. The angle of attack was then increased until (a) flutter was noted, (b) excessive static stresses or vibrations were encountered, or (c) a maximum angle of 19.5° was reached. The model was under continuous observation in order to prevent its failure and the observer made notes concerning its behavior. These notes are the basis for classifying flutter conditions as being mild or severe. When steady flutter occurred the frequency was determined and in some instances a motion-picture record was taken. The angle of attack was then decreased to zero, the aspect ratio was increased by 0.33, and the procedure was repeated. Motion-picture records were taken of 21 cases of intermittent flutter at low angles of attack; at high angles of attack, 25 steady stall-flutter conditions were recorded.

The maximum allowable angles of attack were estimated on the basis of static wing loads and a yield strength of 70,000 lb/sq in. for steel and 40,000 lb/sq in. for aluminum. These limits were not rigidly adhered to and were subject to change during the test at the discretion of the observer.

The effectiveness of the wing clamp was checked by retesting observed stall-flutter conditions (i.e., M, A, α_f) while the wing clamp was rigidly bolted. The angles of attack at which stall flutter occurred with the wing clamp bolted were the same as those when the clamp was actuated by the air cylinder.

RESULTS AND DISCUSSION

The results of the tests are presented in figures 3 to 9 for all wings tested. No flutter was obtained for aspect ratios other than those indicated in the figures. All flutter data presented represent either steady or intermittent flutter as indicated by a steady or intermittent Lissajous pattern on the oscilloscope.

In some instances (fig. 4(a)) where mild flutter was noted at $\alpha = 0^\circ$, the vibrations ceased with but a moderate increase in angle of attack and reappeared at higher angles as stall flutter. Where the flutter was more violent, particularly for the higher aspect ratios of wings 2S and 2A (figs. 3 and 4), the vibrations persisted to higher angles of attack and limited the investigation to the angles shown. It was not possible to establish a definite boundary between classical and separation-type flutter in all instances. Only the steady flutter (figs. 3 to 9) at high angles of attack and the flutter which occurred initially at low angles (0° to 2°) were considered to be subject to classification as stall flutter and low-angle-of-attack flutter, respectively.

Flutter at Low Angles of Attack

The determination of specific flutter points at low angles was not as decisive as was the case at high angles. The motion pictures taken during the tests indicated that the flutter of wings 2A and 2S at small angles of attack was of the coupled bending-torsion type in some instances; however, the predominant frequency was of the order of the first natural bending frequency. The vibrations of wing 2A (fig. 4) were quite severe from Mach number 0.80 to 1.10 for aspect ratios of 2.33 and 2.67. The vibrations were very violent and of large amplitude for aspect ratio 3.00 and the predominant frequency from Mach number 0.85 to 1.00 was approximately 50 cycles per second. The model failed at $M = 1.02$, $A = 3.00$ as the tunnel speed was being reduced. The failure is believed to have been a result of structural fatigue rather than of divergent flutter since the model appeared to be more stable at Mach numbers above 1.00.

The intermittent flutter noted for wing 2S (fig. 3) was near the first natural bending frequency for aspect ratios 2.67 to 3.33. The vibrations for aspect ratios 3.67 and 4.00 became progressively more severe with increasing Mach number, so that the Mach number was limited to 0.94. No flutter frequencies were determined for these aspect ratios.

The vibrations of wing 4AX (fig. 7) at low angles were also near the first natural bending frequency for aspect ratios of 3.33, 3.67, and 4.00 and did not appear to be in a coupled mode at any time. The vibrations of this wing when positioned at aspect ratios greater than 4.00 were too erratic to determine the frequency.

[redacted]

No low-angle-of-attack flutter was encountered for wings 4S, 4A, 6A, or 6AX. The intermittent flutter at moderate angles of attack which was noted for wing 4A (fig. 6; A = 3.67, 4.00; $\alpha = 3.5^\circ$) and wing 6A (fig. 8; A = 6.00; $\alpha = 4.5^\circ$) was not considered to be of the low-angle-of-attack type since no flutter occurred at $\alpha \cong 0^\circ$.

Flutter at High Angles of Attack

The stall flutter was of a steady torsional mode at or near the first natural torsional frequency of the wing, a phenomenon which substantiates results of previous investigations. The predominant torsional mode was clearly evident in the motion pictures for various stall-flutter conditions. At a given Mach number, the intensity of the vibrations generally increased with angle of attack to the limits of the test. However, for wing 2S at A = 1.67 (fig. 3), it was possible to increase the angle of attack until a stable condition was again established.

Several of the wings tested appeared to be less susceptible to stall flutter at the higher test Mach numbers. This trend was particularly evident in the case of wing 4AX (fig. 7; A = 2.00) for which steady flutter occurred at M = 0.90 ($\alpha = 16.5^\circ$), intermittent flutter occurred at M = 0.94 ($\alpha = 15.5^\circ$ to 19.5°), and no flutter was noted from M = 0.98 to M = 1.10 at angles of attack up to 19.5°. A similar but less pronounced trend was noted for this wing at A = 2.33 and 2.67, as well as for wing 6AX (fig. 9; A = 3.33 to 4.67), and wing 2S (fig. 3; A = 1.67).

As mentioned previously, the occurrence of steady stall flutter was pronounced and easily determined by the Lissajous patterns on the oscilloscope. The minimum angle of attack at which steady flutter occurred (α_f) has, therefore, been plotted as a function of Mach number in figures 10(a) to 15(a) to summarize the effects of Mach number and aspect ratio for all wings except 6A. This wing exhibited only a mild form of intermittent flutter within the angle-of-attack range investigated.

Data from part (a) of figures 10 to 15 are presented in a different form in part (b) of these figures to introduce the conventional flutter parameter $V/b\omega_\alpha$ as a function of α_f. The parameter $V/b\omega_\alpha$ decreased rapidly with increasing angle of attack. A value of $V/b\omega_\alpha \cong 1$ has been suggested in reference 2 as being useful in estimating the minimum stall-flutter velocity of thin wings. Explicit verification of this criterion is not possible, however, since no data were taken at Mach numbers less than 0.60 or at angles greater than 19.5°.

In figure 16, α_f is plotted as a function of aspect ratio at M = 0.60 to indicate the effect of a reduction in torsional stiffness on α_f for the 4-percent and 6-percent aluminum wings. As noted previously, wing 6A exhibited only mild intermittent flutter up to the maximum

angles of attack allowable from mechanical or strength considerations. These values of α, shown in figure 16 for this wing, are considered to be conservative estimates of the true values of α_f. The data as presented indicate that reduction of torsional stiffness had a more pronounced effect for the 6-percent wing than for the 4-percent wing. A similar comparison at other Mach numbers is not possible, however, because of the lack of data for the solid wings. Wing 4A failed during the test before sufficient stall-flutter data were obtained. The data for wing 6A at Mach numbers higher than 0.60 were not deemed sufficiently reliable to continue the comparison.

Stall flutter has been associated in the past with the static lift curve (see ref. 4). This association led the authors of reference 4 to suggest three possible causes of stall flutter: (1) static instability due to the negative slope of the lift curve at angles beyond the stall, (2) dynamic instability due to hysteresis at the stall, and (3) instability resulting from Kármán vortex excitation.

In figures 17, 18, and 19 the angles of attack at which flutter was observed have been noted on static lift curves taken from reference 5. These static data were obtained from tests conducted in the same facility and on models of the same size as those of the subject investigation. It must be noted, however, that these curves are for wings having symmetrical NACA 63A-series sections rather than the 64A-series used in the present investigation. Comparison of available 63-series and 64-series-airfoil-section data in references 6, 7, and 8 indicates that the static data used are indicative of the true static characteristics.

The limited number of available data as shown in figures 17 to 19 indicate that with respect to the three possible causes of stall flutter cited above, only the steady flutter of wing 4AX at the lower aspect ratios (fig. 18) and the intermittent flutter of wing 6A, A = 6.00 (fig. 19) may be attributed to static instability due to the negative slope of the lift curve. The remaining cases of steady flutter can then be considered as probably being a result of the hysteresis loop described by the lift curve since the stall-flutter frequencies were considerably lower than the vortex frequencies calculated by the method given in reference 4.

CONCLUDING REMARKS

Flutter at low angles of attack occurred only for the 2-percent-thick steel and aluminum wings and for a 4-percent-thick aluminum wing slotted spanwise to reduce the torsional stiffness. The predominant flutter frequency was of the order of the first natural bending frequency.

Stall flutter occurred at frequencies which were in good agreement with the experimentally determined first natural torsional frequencies.

The angles of attack at which stall flutter occurred have been indicated on the static lift curves of a series of rectangular wings having symmetrical NACA 63A-series sections. In the majority of cases, flutter occurred at angles below those for maximum lift.

Ames Aeronautical Laboratory
National Advisory Committee for Aeronautics
Moffett Field, Calif., Jan. 29, 1954

REFERENCES

1. Martin, Dennis J.: Summary of Flutter Experiences as a Guide to the Preliminary Design of Lifting Surfaces on Missiles. NACA RM L51J30, 1951.

2. Rainey, A. Gerald: Preliminary Study of Some Factors Which Affect the Stall-Flutter Characteristics of Thin Wings. NACA RM L52D08, 1952.

3. Myklestad, Nils O.: Vibration Analysis. McGraw-Hill Book Co., Inc., 1944, p. 162.

4. Bollay, William, and Brown, Charles D.: Some Experimental Results on Wing Flutter. Jour. Aero. Sci., vol. 8, no. 8, June 1941, pp. 313-318.

5. Nelson, Warren H., and McDevitt, John B.: The Transonic Characteristics of 17 Rectangular, Symmetrical Wing Models of Varying Aspect Ratio and Thickness. NACA RM A51A12, 1951.

6. Ilk, Richard J.: High-Speed Aerodynamic Characteristics of Four Thin NACA 63-Series Airfoils. NACA RM A7J23, 1947.

7. Wilson, Homer B., Jr., and Horton, Elmer A.: Aerodynamic Characteristics at High and Low Subsonic Mach Numbers of Four NACA 6-Series Airfoil Sections at Angles of Attack from -2° to 31°. NACA RM L53C20, 1953.

8. Loftin, Lawrence K., Jr.: Theoretical and Experimental Data for a Number of NACA 6A-Series Airfoil Sections. NACA Rep. 903, 1948.

TABLE I.- CHARACTERISTICS OF THE WINGS TESTED

Wing designation	Wing section	Material	Mass density ratio, μ	Dimensionless radius of gyration, r_α	Bending stiffness, EI, lb-in.^{2}	Torsional stiffness, GJ, lb-in.^{2}	$x_{e.a.}$, percent chord	$x_{c.g.}$, percent chord
2S	64A002	Steel	108	0.460	1.15×10^4	1.84×10^4	37.3	43.5
2A	64A002	Aluminum	38	.499	0.403	0.594	38.3	43.5
4S	64A004	Steel	216	.410	9.24	14.77	40.0	43.5
4A	64A004	Aluminum	76	.409	3.23	4.77	43.3	43.5
[1]4AX	64A004	Aluminum	76	.571	3.23	3.51	43.5	43.5
6A	64A006	Aluminum	114	.425	10.92	16.1	46.0	43.5
[2]6AX	64A006	Aluminum	114	.547	10.92	10.6	40.5	43.5

[1]Spanwise slots having a depth of 55 percent of the wing-section ordinate located at chordwise intervals of 0.3 inch between 5- and 90-percent chord.

[2]Spanwise slots having a depth of 35 percent of the wing-section ordinate located at intervals of 0.3 inch between 5- and 90-percent chord.

Note: Values of mass density ratio μ are based on the density of air at sea level. For variation of test density with Mach number see figure 2.

TABLE II.- STILL-AIR FORCED-VIBRATION CHARACTERISTICS OF WINGS TESTED

Wing	Aspect ratio									
	2		3		4		5		6	
	[1,2]$b\omega_h$	[3]$b\omega_\alpha$	[1,2]$b\omega_h$	[3]$b\omega_\alpha$	[1,2]$b\omega_h$	[3]$b\omega_\alpha$	[1,2]$b\omega_h$	[3]$b\omega_\alpha$	[1,2]$b\omega_h$	[3]$b\omega_\alpha$
2S	117.8	323.5	55.2	213.5	34.1	158.5	- - -	- - -	- - -	- - -
2A	119.5	311.0	56.6	207.0	35.3	152.4	- - -	- - -	- - -	- - -
4S	- - -	- - -	94.2	436.0	59.8	342.0	41.0	278.0	29.2	231.0
4A	- - -	- - -	92.6	432.0	55.8	316.0	38.0	262.0	28.8	220.0
4AX	263.0	575.0	116.8	383.0	66.7	284.0	48.2	228.0	37.2	195.0
6A	- - -	- - -	152.4	644.0	88.8	474.0	60.0	400.0	42.6	330.0
6AX	- - -	- - -	157.8	534.0	91.1	393.0	60.0	311.0	45.4	259.0

[1]b wing semichord, 0.25 ft.
[2]ω_h first natural bending frequency, radians/sec.
[3]ω_α first natural torsional frequency, radians/sec.

NACA

TABLE III.- EXPERIMENTALLY DETERMINED STRUCTURAL DAMPING COEFFICIENTS

Wing	Aspect ratio									
	2		3		4		5		6	
	[1]g_h	[2]g_α	[1]g_h	[2]g_α	[1]g_h	[2]g_α	[1]g_h	[2]g_α	[1]g_h	[2]g_α
2S	0.008	0.003	0.007	- - -	0.005	0.004	- - -	- - -	- - -	- - -
4S	- - -	- - -	- - -	0.004	.005	.003	0.006	- - -	- - -	- - -
4A	- - -	- - -	.013	.004	.007	.004	.006	- - -	0.005	- - -
4AX	- - -	- - -	.007	- - -	.006	- - -	- - -	- - -	.007	- - -

[1]g_h structural damping coefficient for the bending mode.
[2]g_α structural damping coefficient for the torsion mode.

NACA

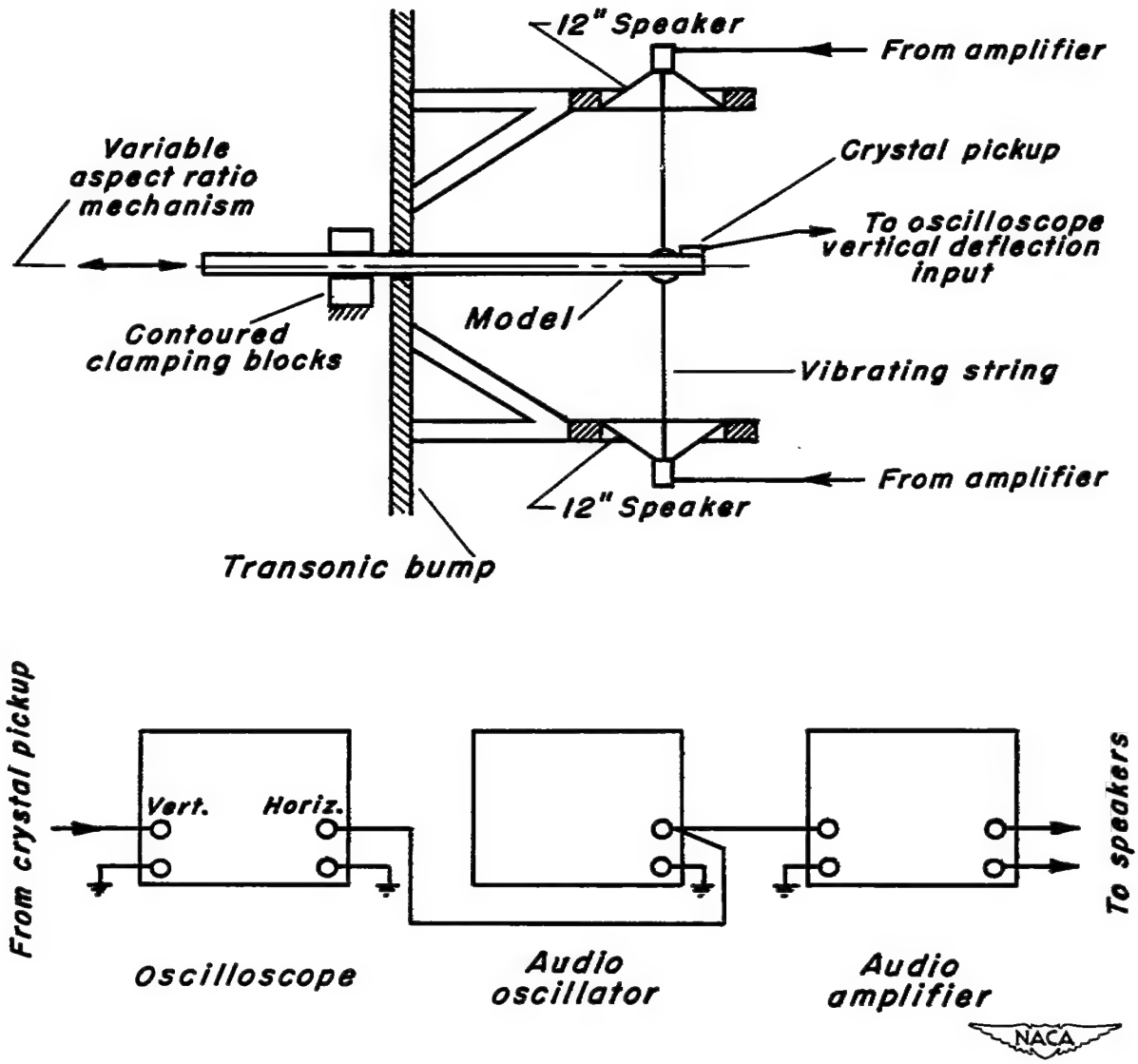

Figure 1.- Schematic and block diagrams of apparatus used for the determination of the natural frequencies.

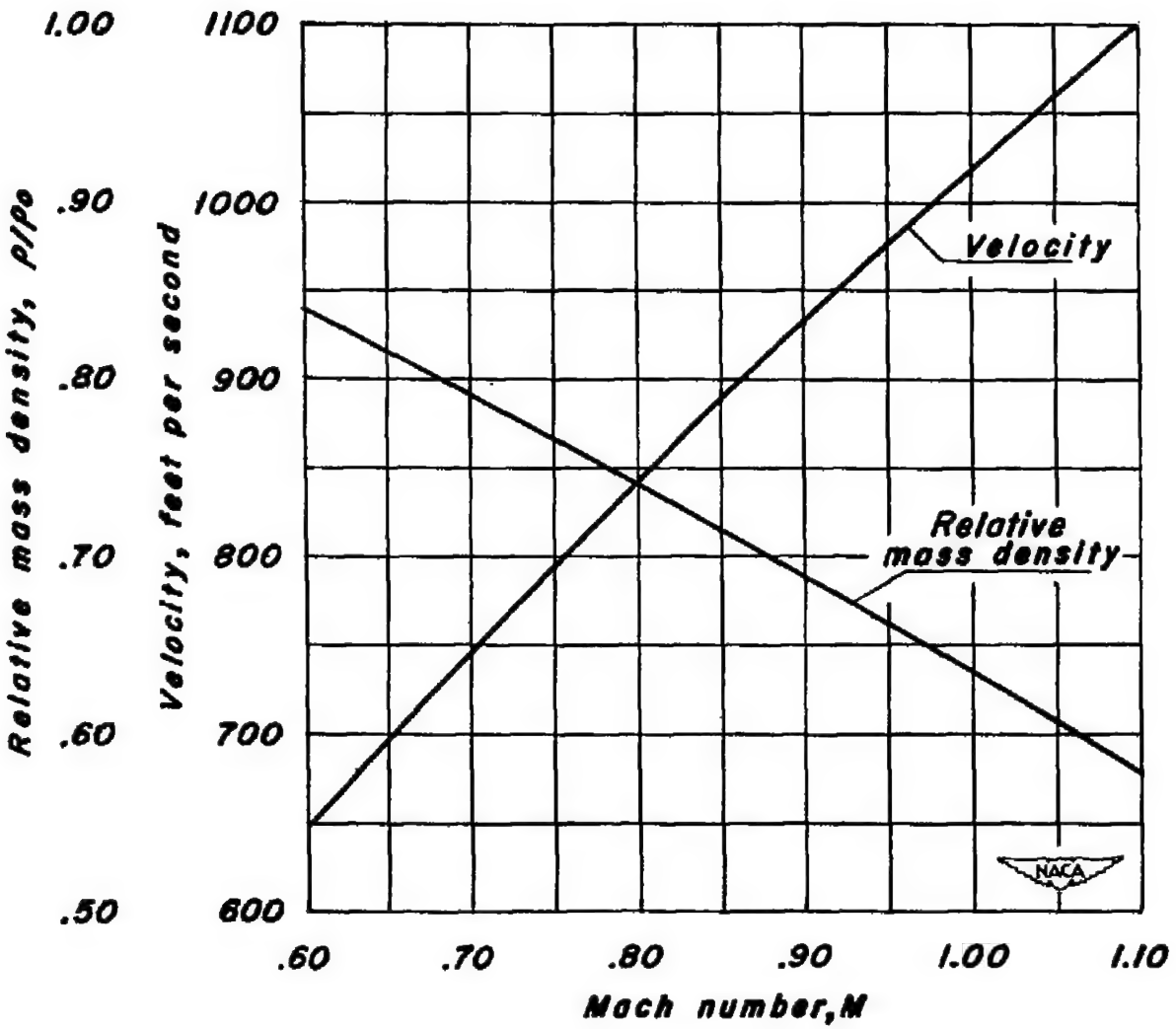

Figure 2.- Variation of velocity and relative density with Mach number.

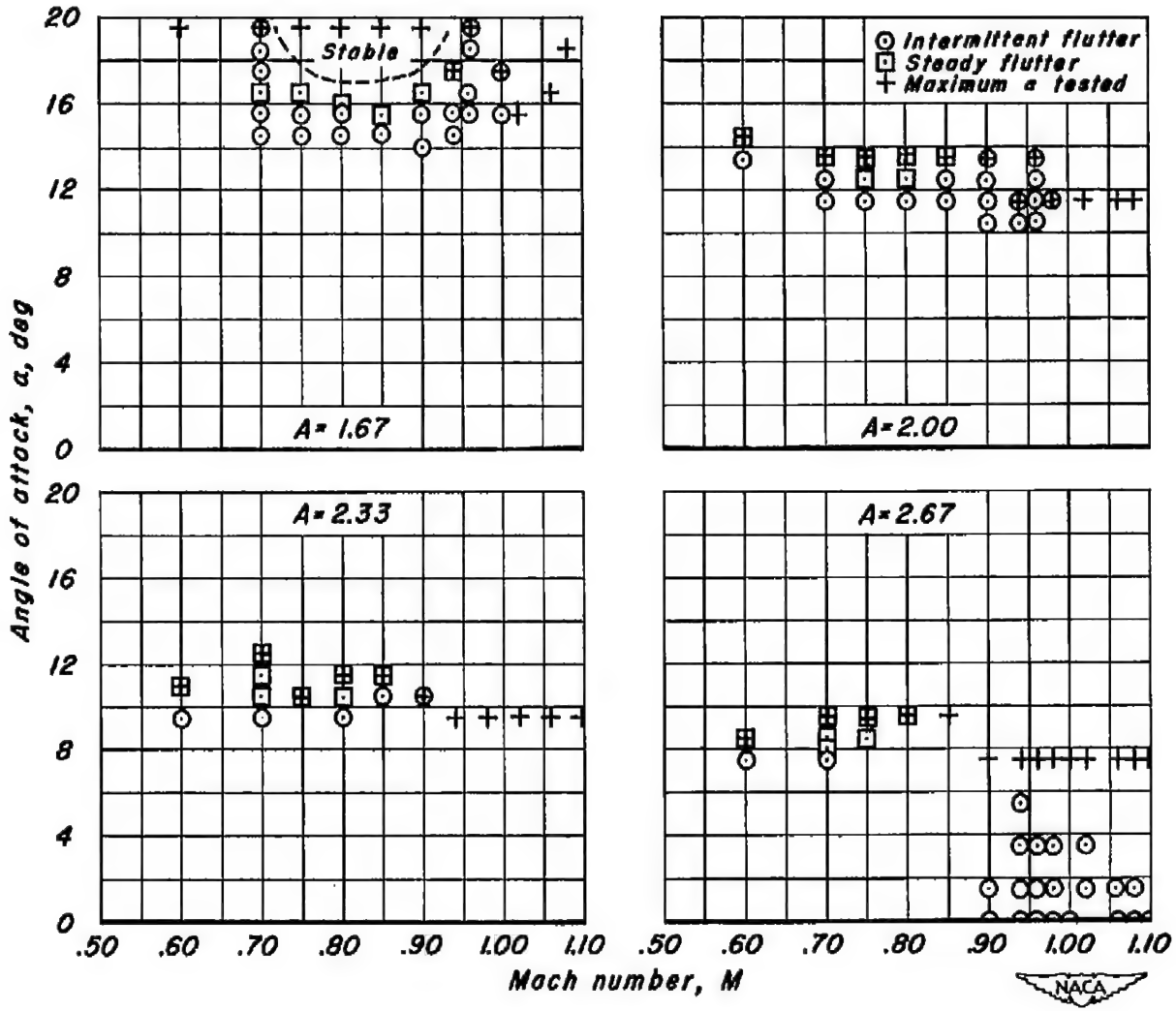

(a) A = 1.67, 2.00, 2.33, 2.67

Figure 3.- Flutter observations, wing 2S.

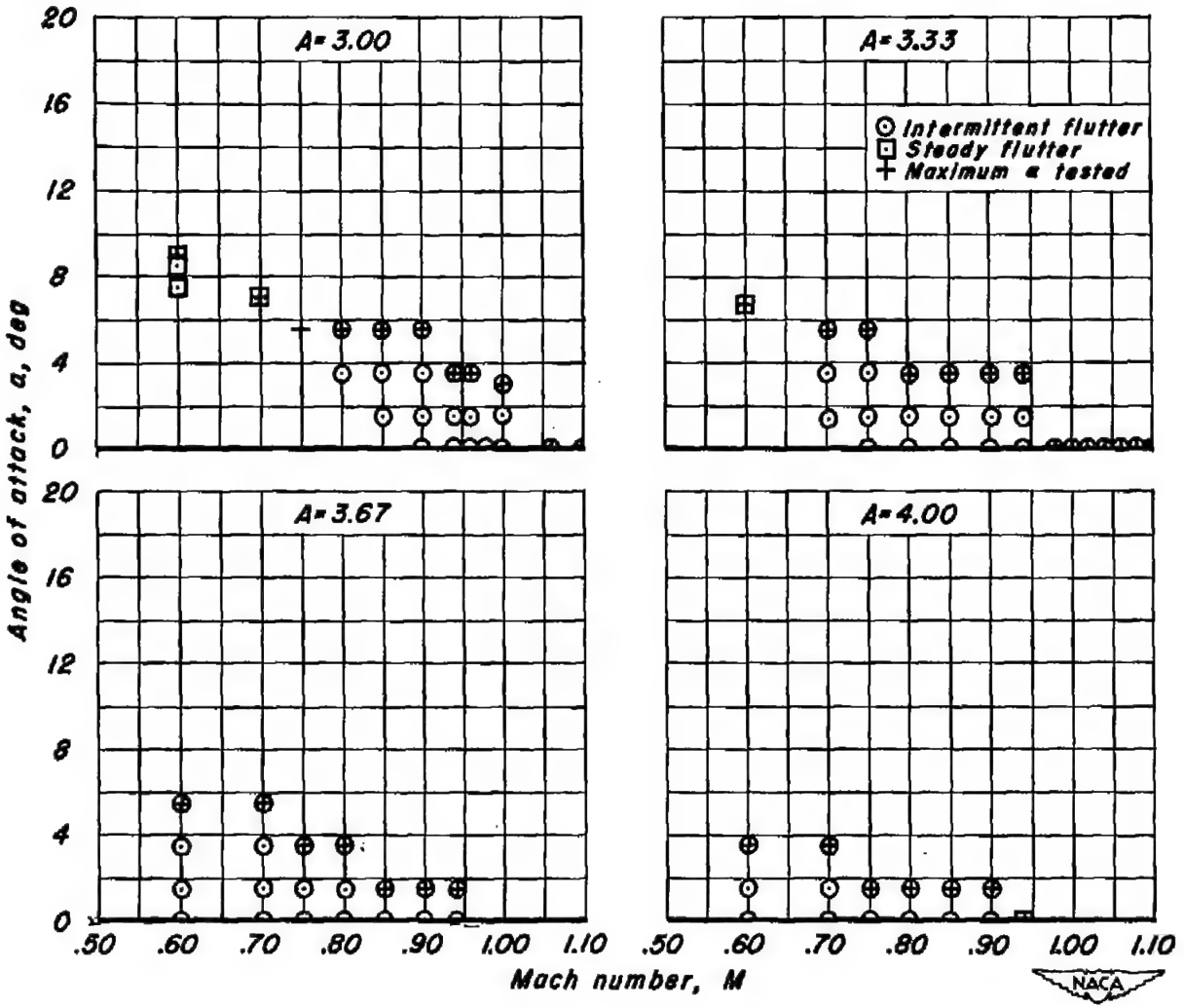

(b) A = 3.00, 3.33, 3.67, 4.00

Figure 3.- Concluded.

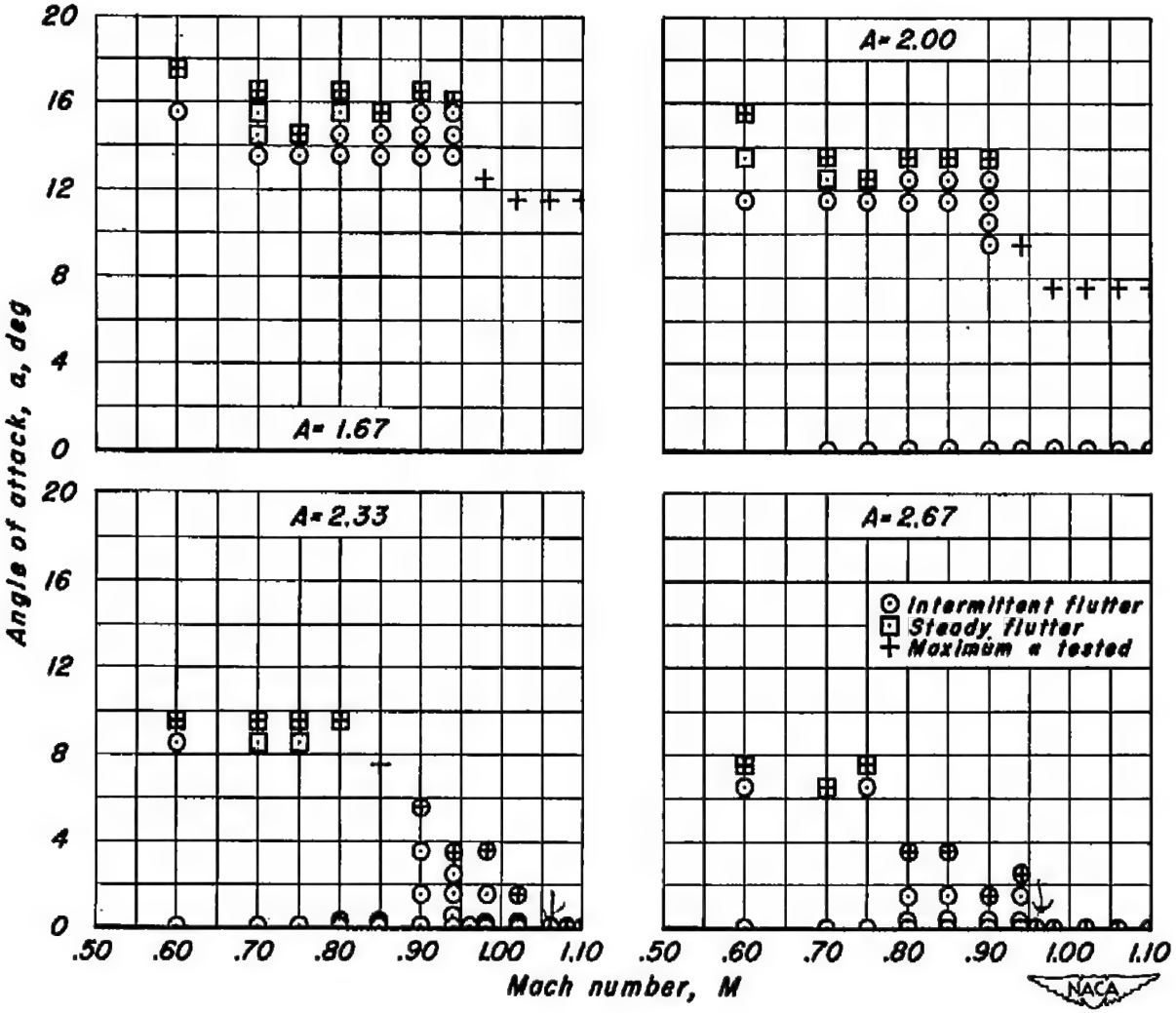

(a) A = 1.67, 2.00, 2.33, 2.67

Figure 4.- Flutter observations, wing 2A.

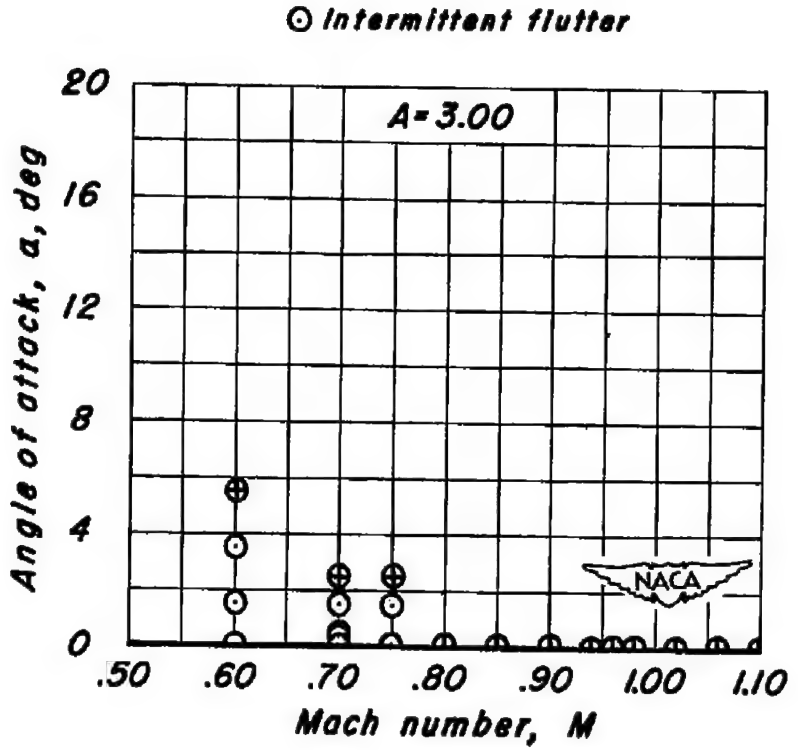

(b) A = 3.00

Figure 4.- Concluded.

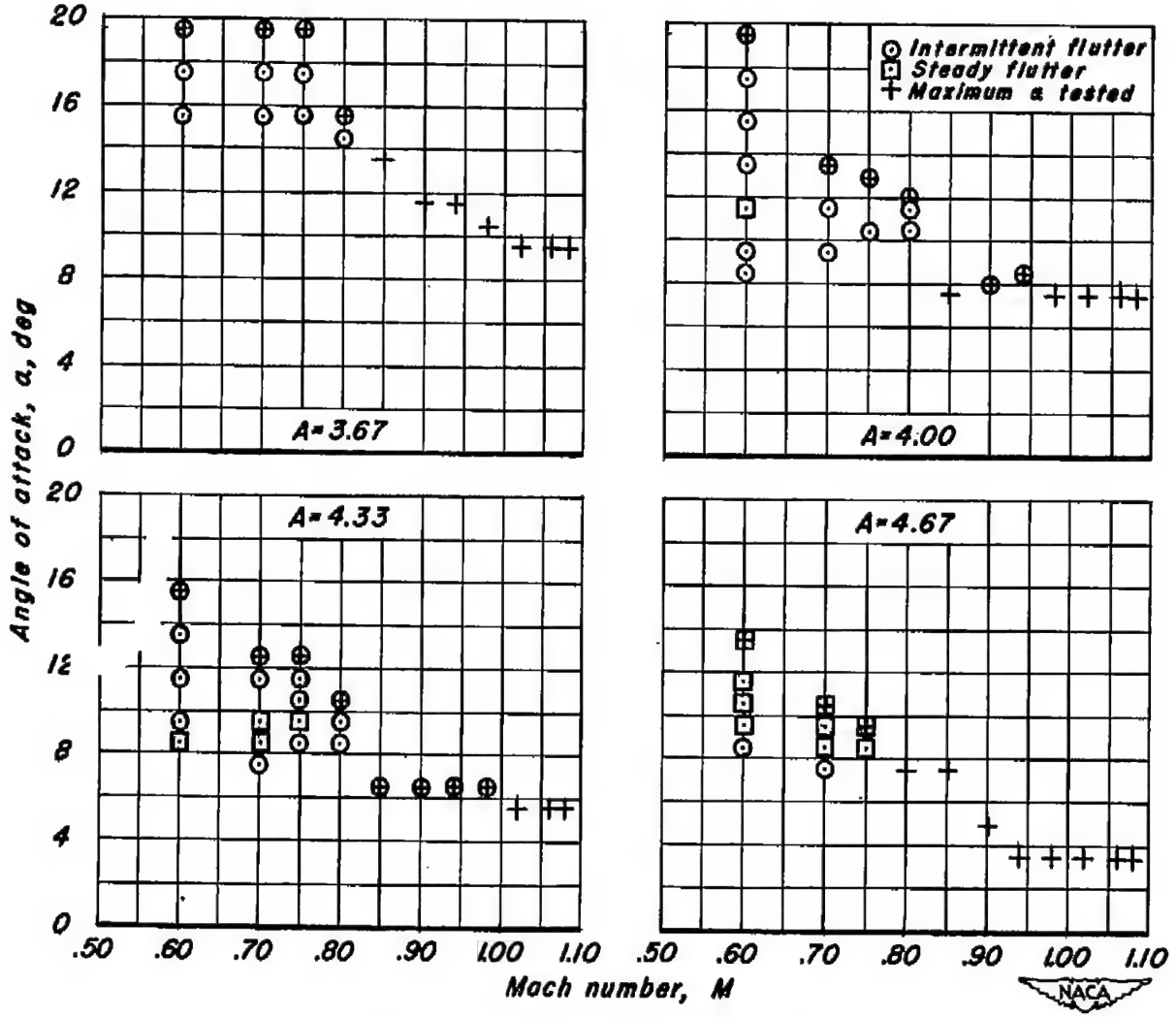

(a) A = 3.67, 4.00, 4.33, 4.67

Figure 5.- Flutter observations, wing 48.

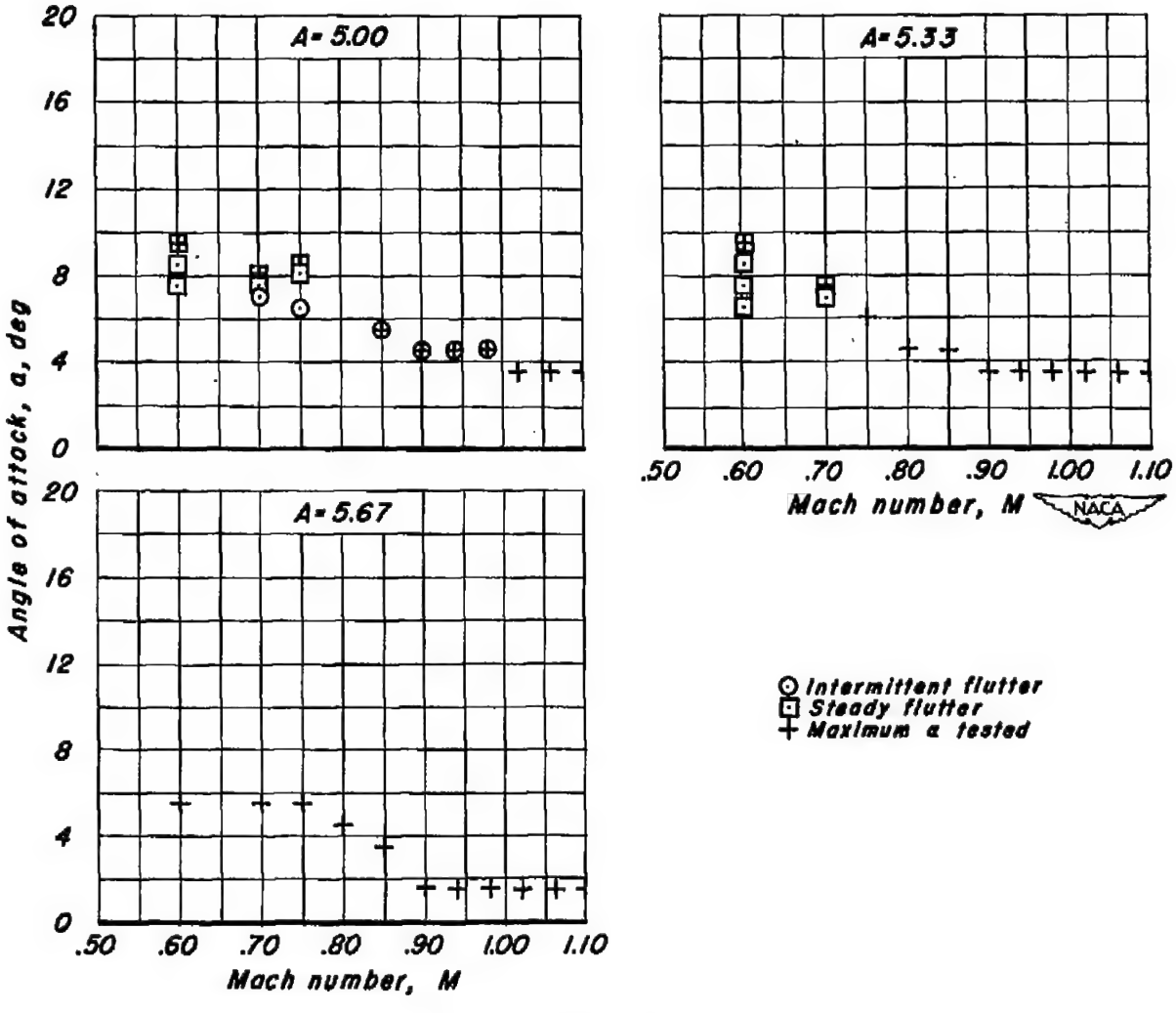

(b) A = 5.00, 5.33, 5.67

Figure 5.- Concluded.

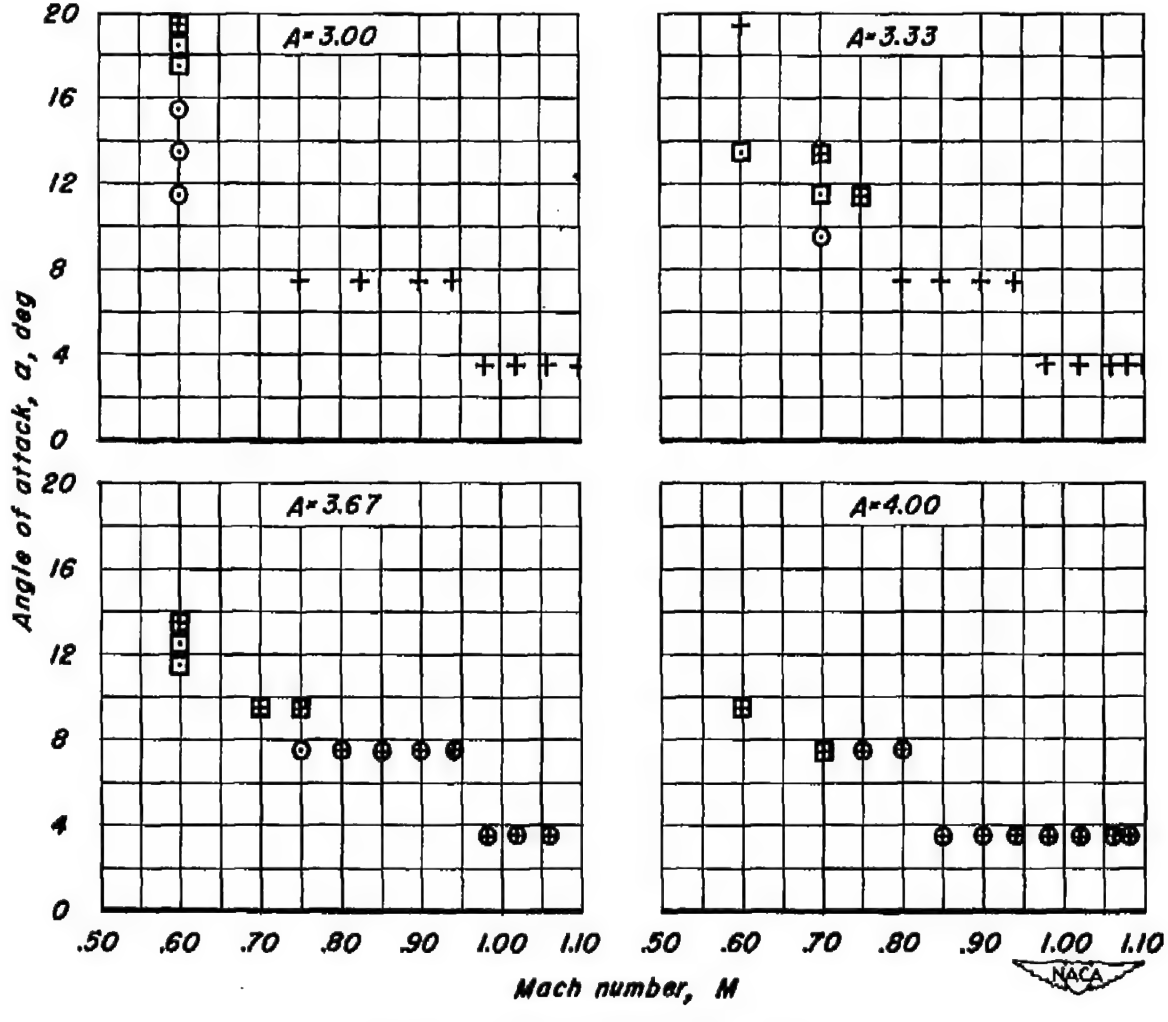

(a) A = 3.00, 3.33, 3.67, 4.00

Figure 6.- Flutter observations, wing 4A.

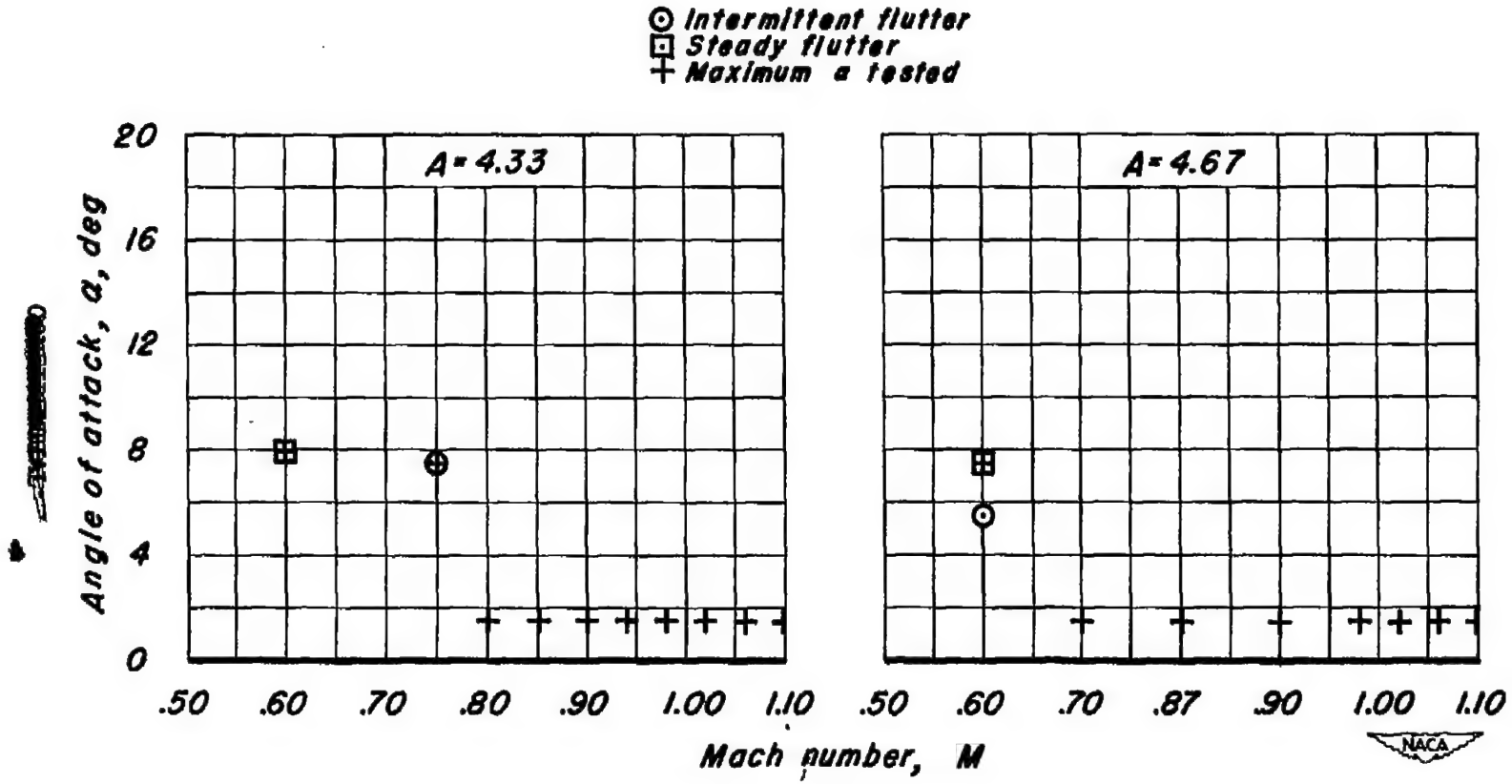

(b) A = 4.33, 4.67

Figure 6.- Concluded.

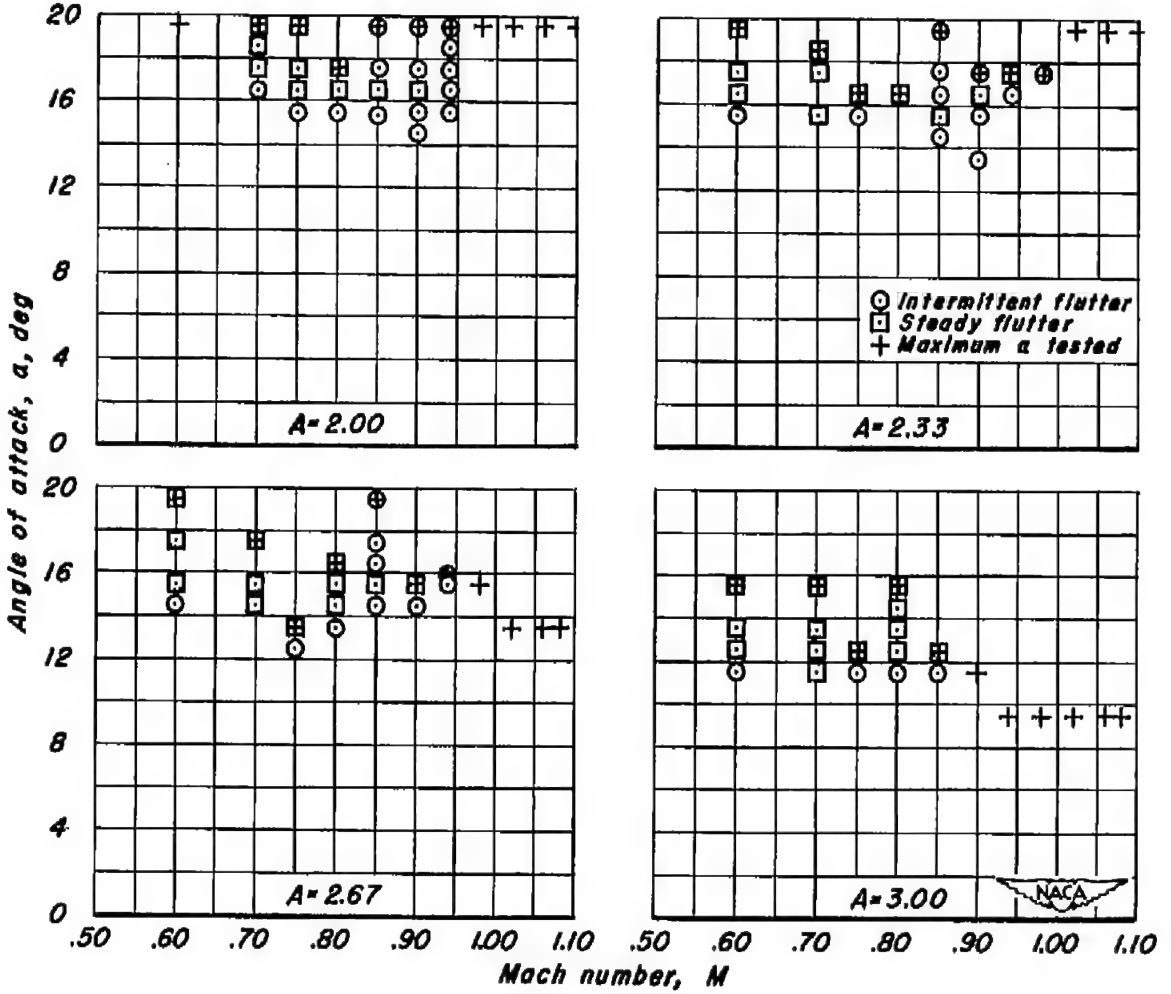

(a) A = 2.00, 2.33, 2.67, 3.00

Figure 7.- Flutter observations, wing 4AX.

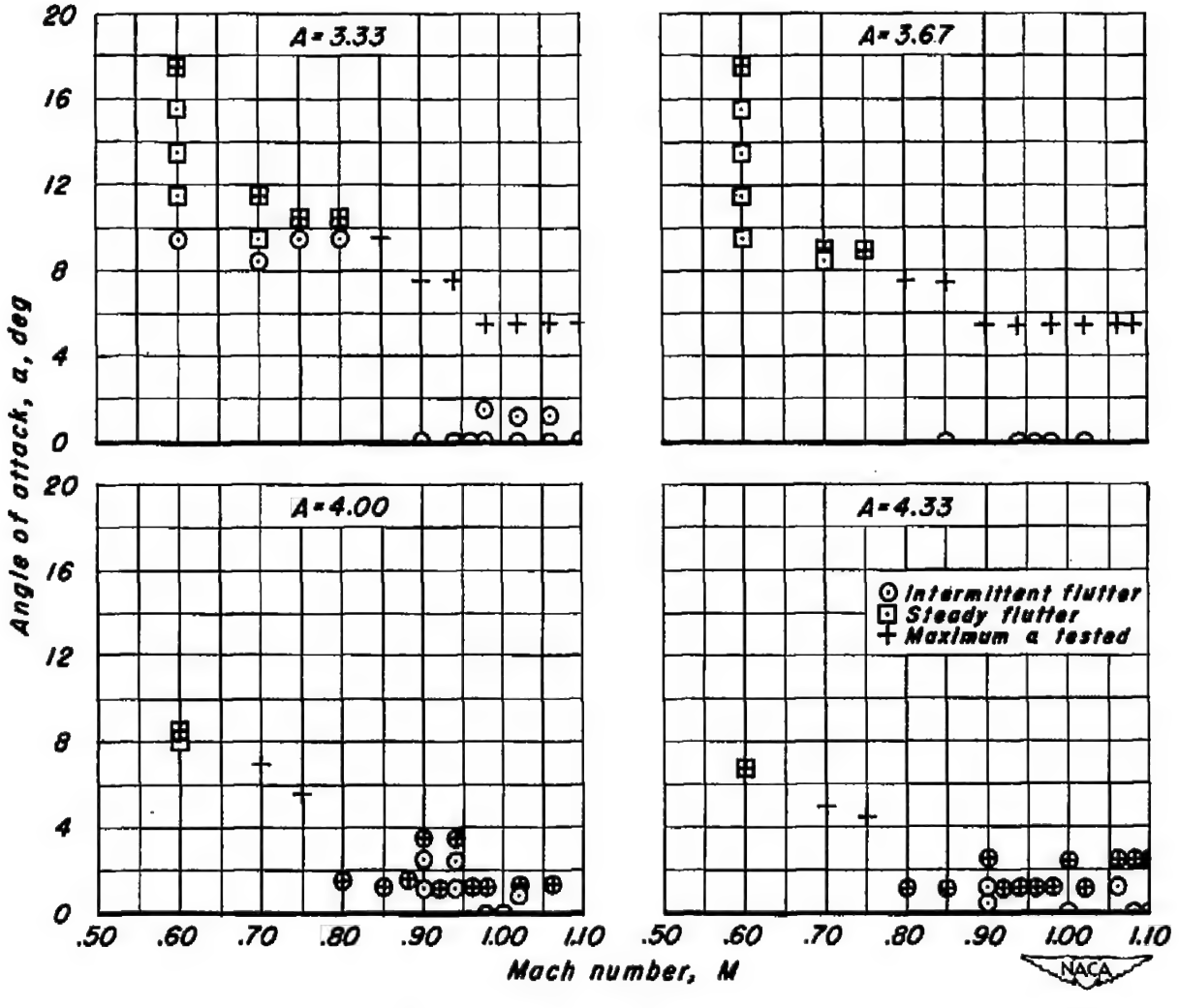

(b) A = 3.33, 3.67, 4.00, 4.33

Figure 7.- Continued.

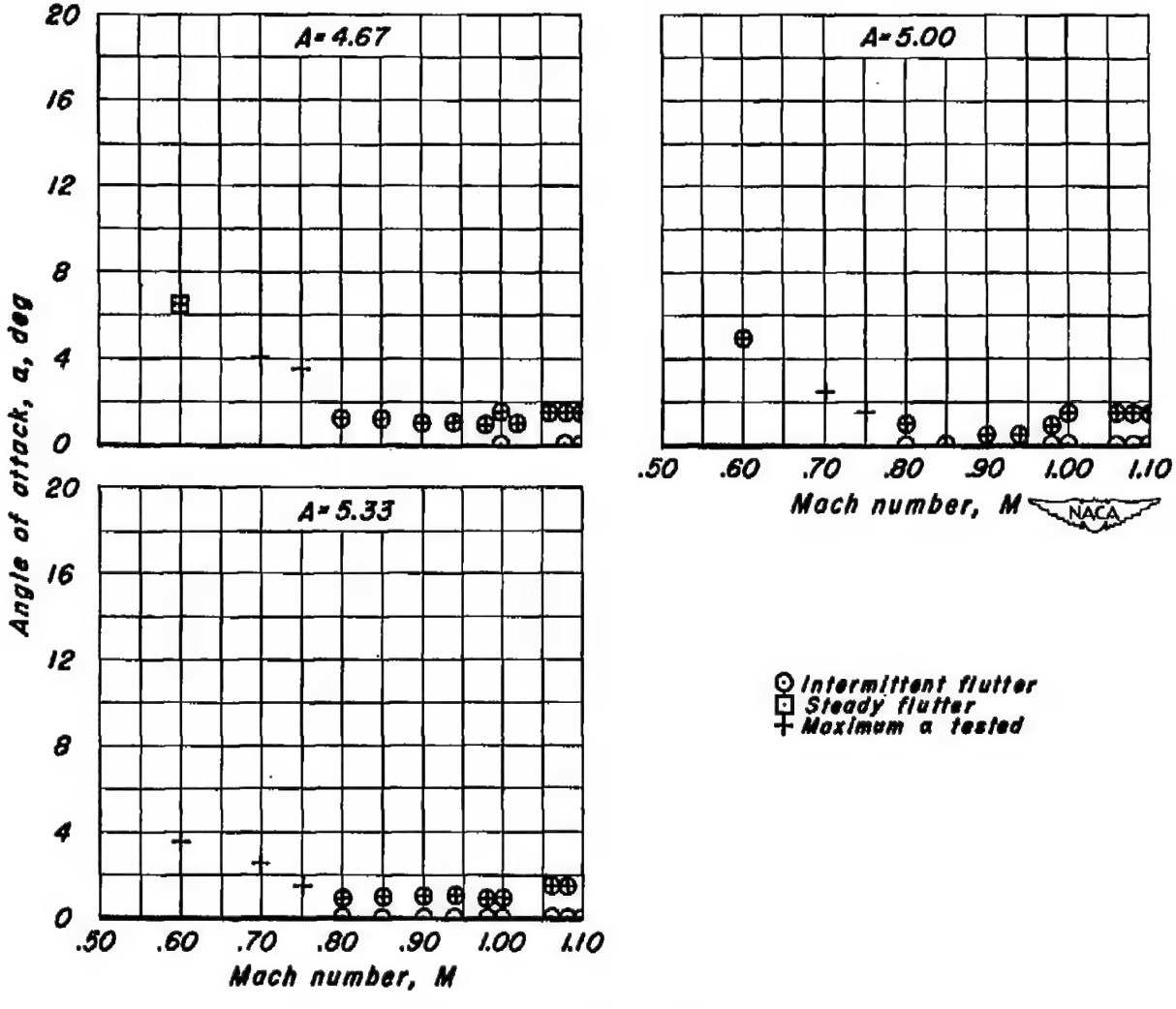

(c) A = 4.67, 5.00, 5.33

Figure 7.- Concluded.

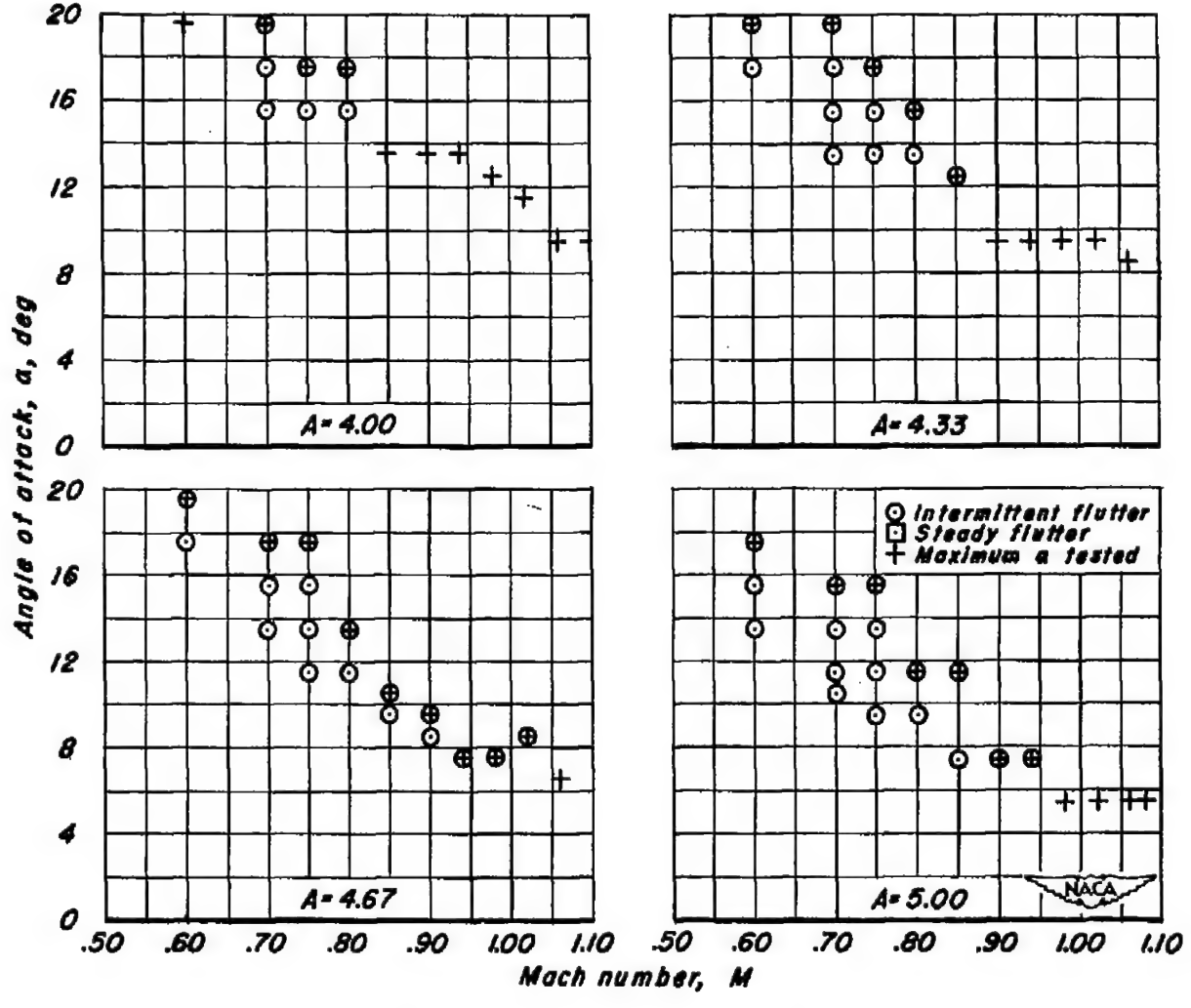

(a) A = 4.00, 4.33, 4.67, 5.00

Figure 8.- Flutter observations, wing 6A.

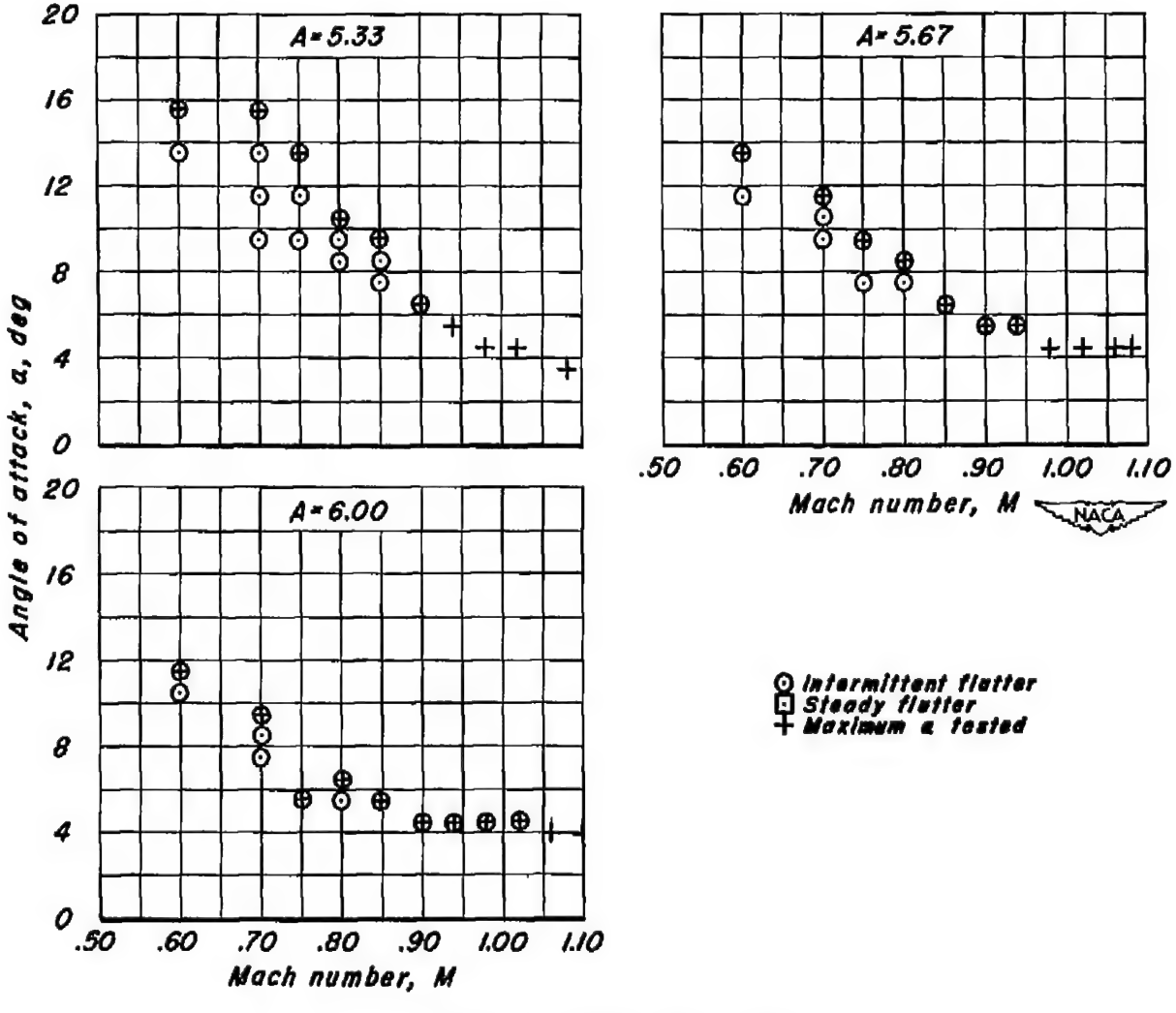

(b) A = 5.33, 5.67, 6.00

Figure 8.- Concluded.

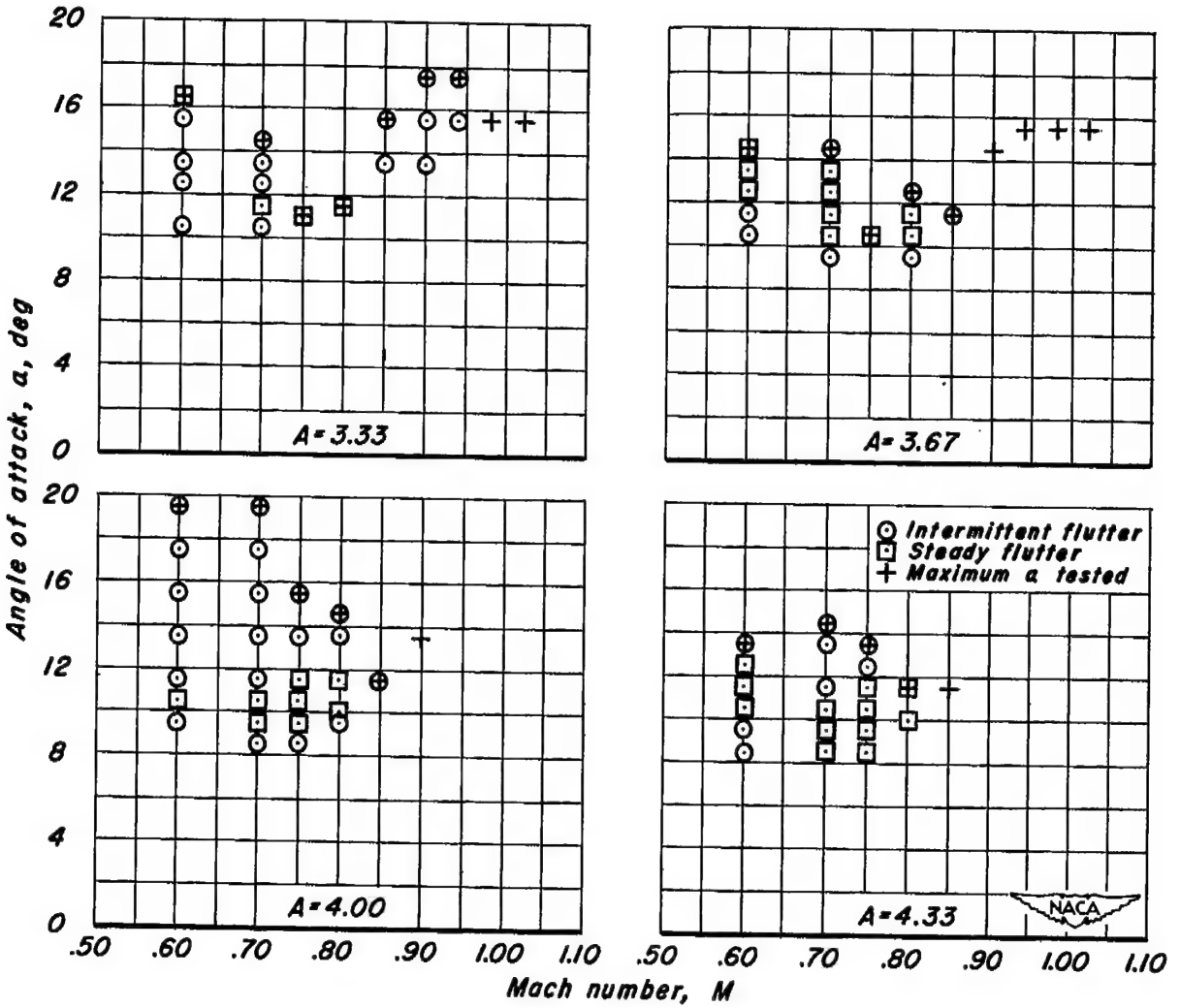

(a) A = 3.33, 3.67, 4.00, 4.33

Figure 9.- Flutter observations, wing 6AX.

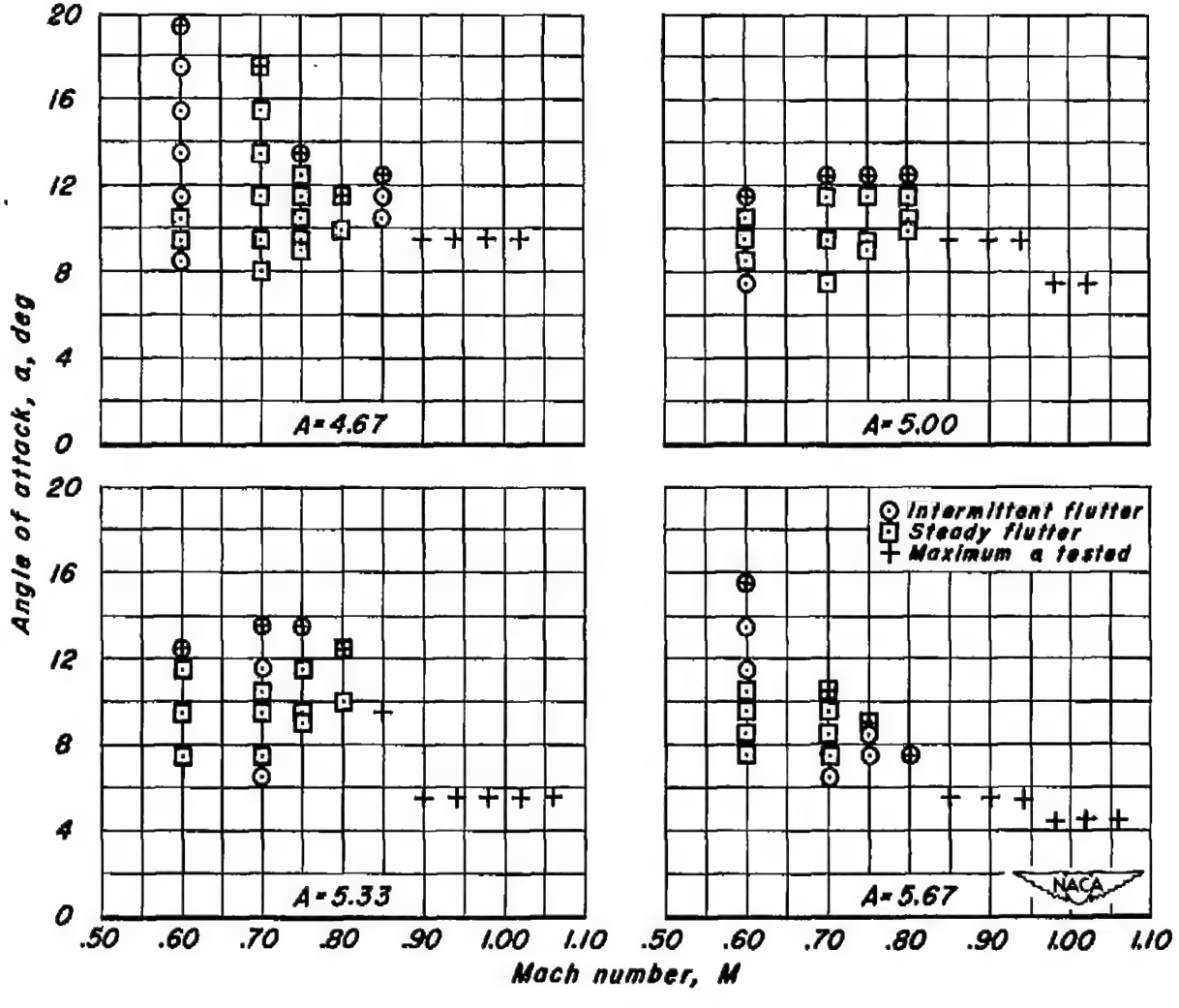

(b) A = 4.67, 5.00, 5.33, 5.67

Figure 9.- Concluded.

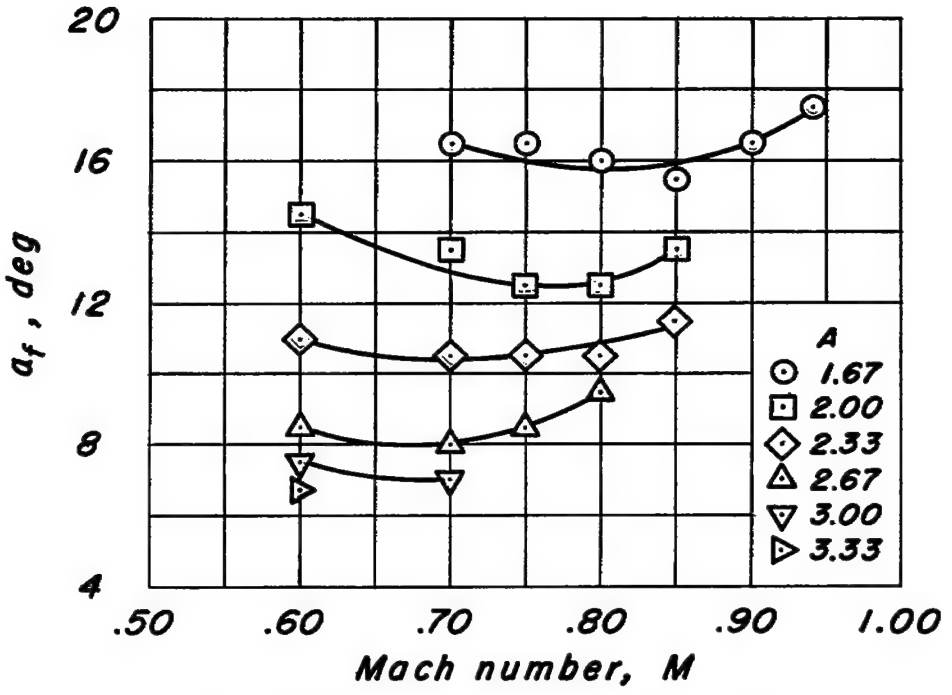

(a) Variation of α_f with Mach number.

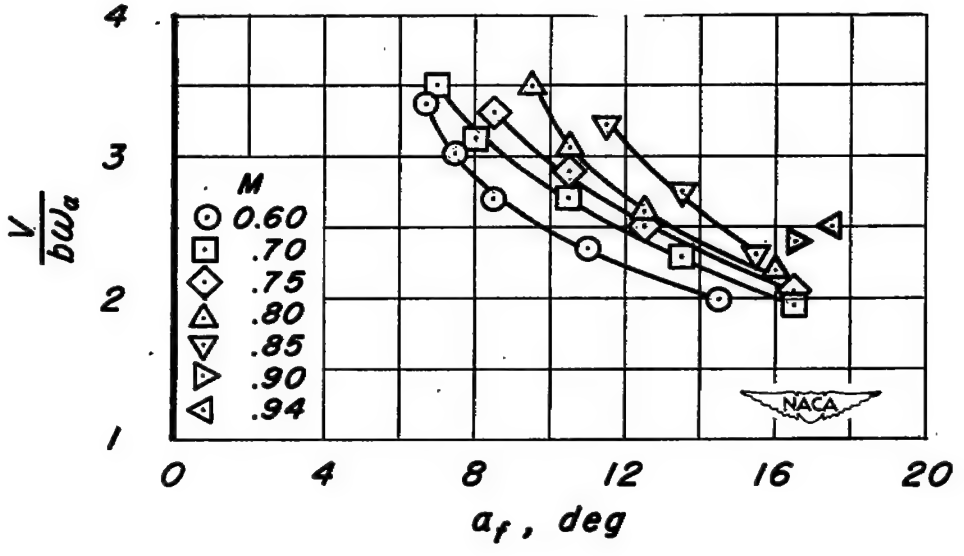

(b) Variation of $\frac{V}{b\omega_\alpha}$ with α_f.

Figure 10.- Effect of aspect ratio and Mach number on the stall flutter of wing 2S.

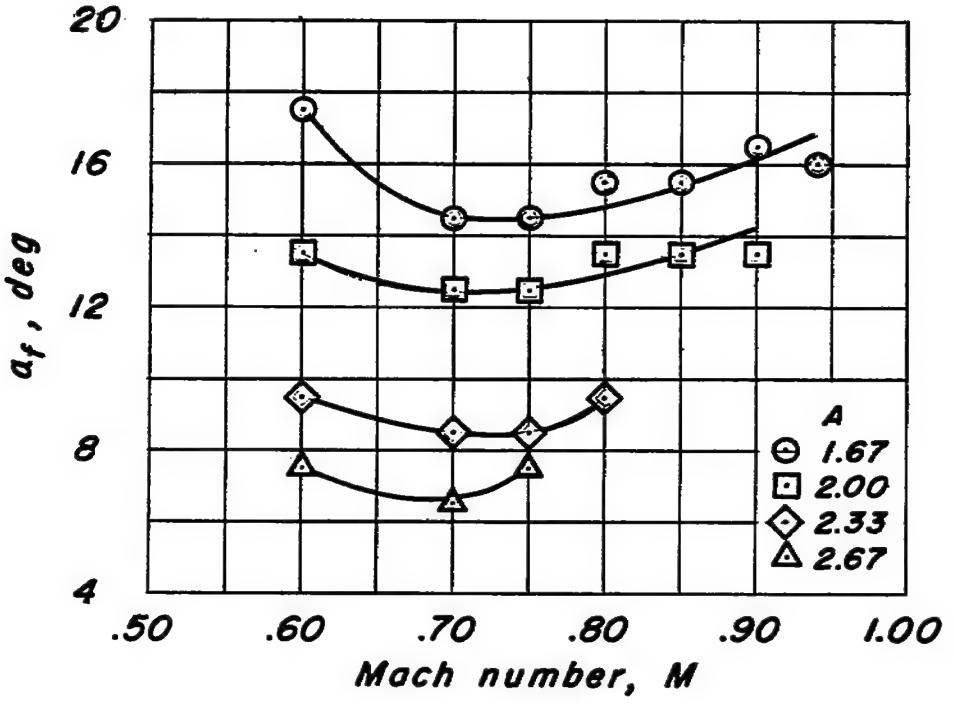

(a) Variation of α_f with Mach number.

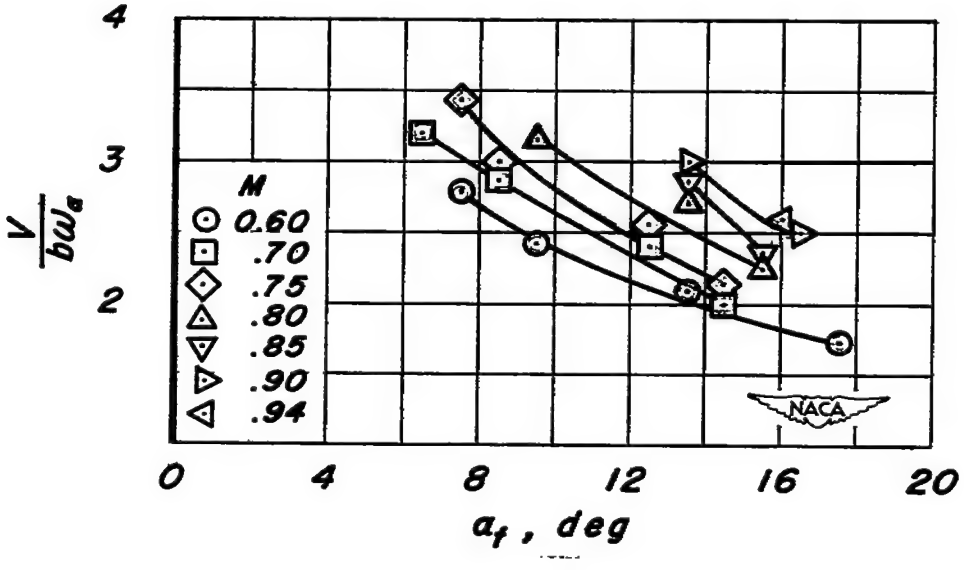

(b) Variation of $\frac{V}{b\omega_\alpha}$ with α_f.

Figure 11.- Effect of aspect ratio and Mach number on the stall flutter of wing 2A.

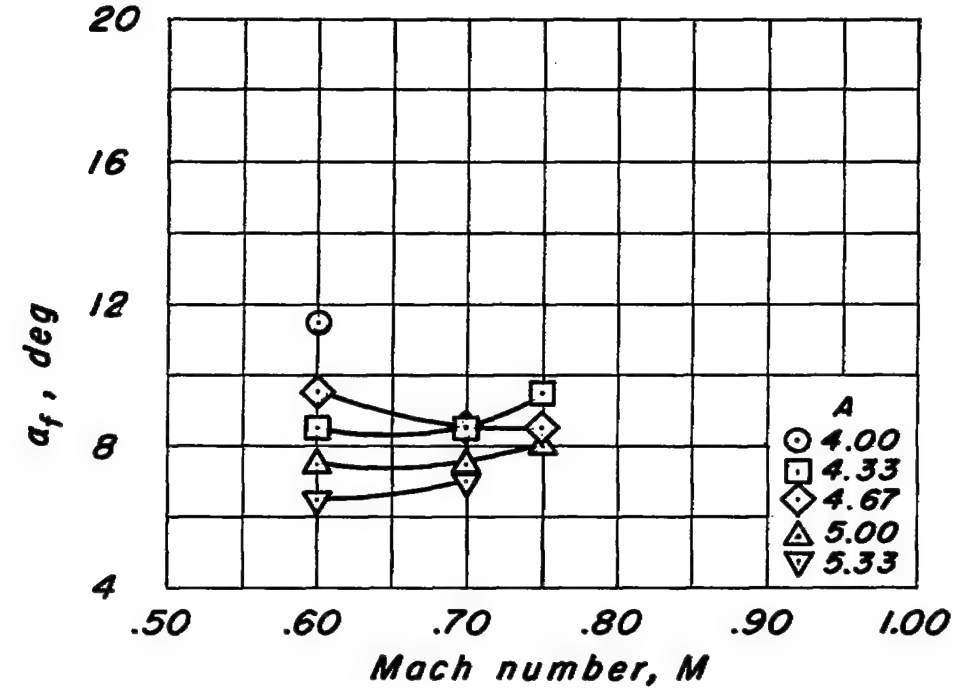

(a) Variation of α_f with Mach number.

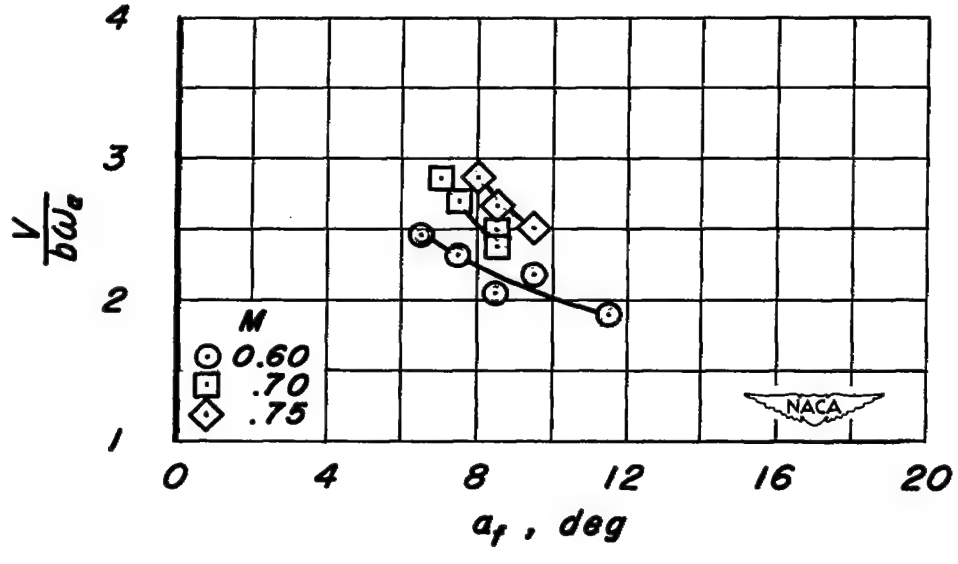

(b) Variation of $\frac{V}{b\omega_\alpha}$ with α_f.

Figure 12.- Effect of aspect ratio and Mach number on the stall flutter of wing 4S.

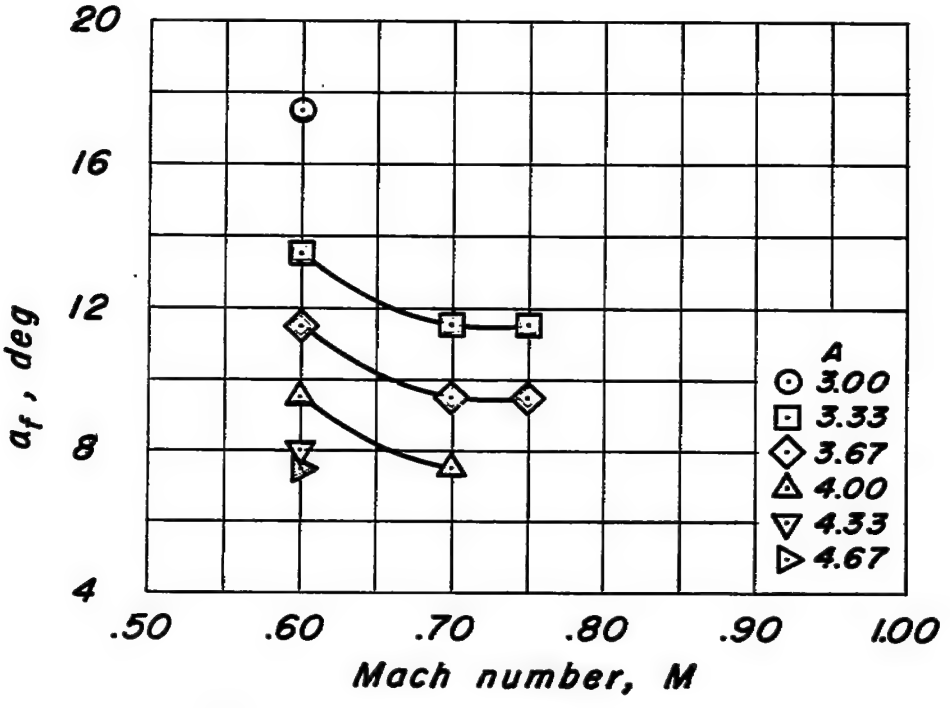

(a) Variation of α_f with Mach number.

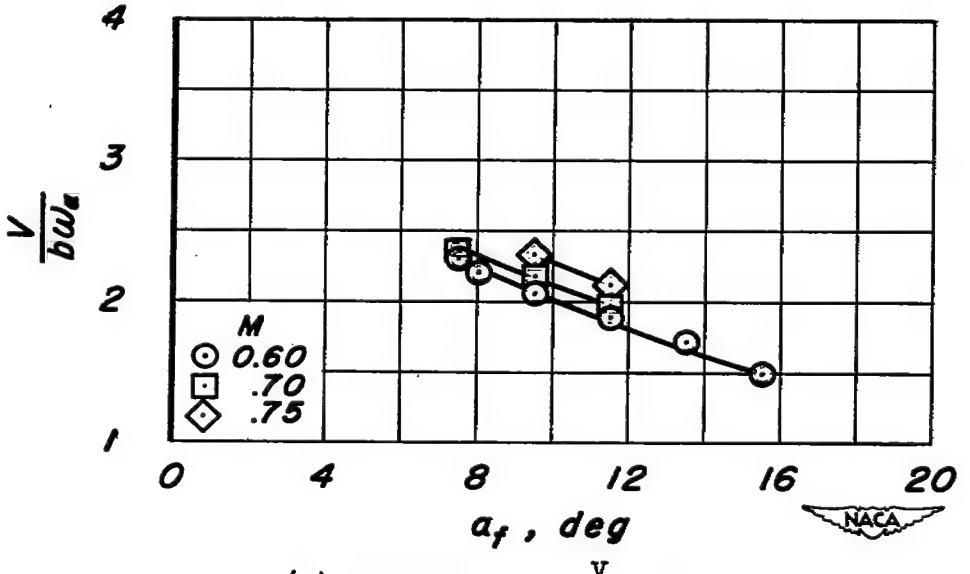

(b) Variation of $\frac{V}{b\omega_\alpha}$ with α_f.

Figure 13.- Effect of aspect ratio and Mach number on the stall flutter of wing 4A.

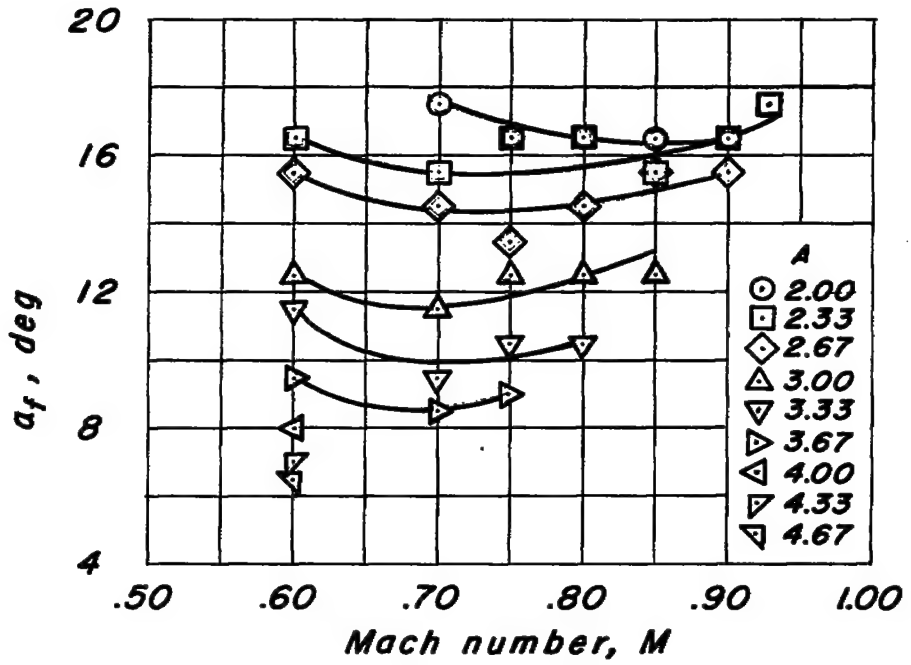

(a) Variation of α_f with Mach number.

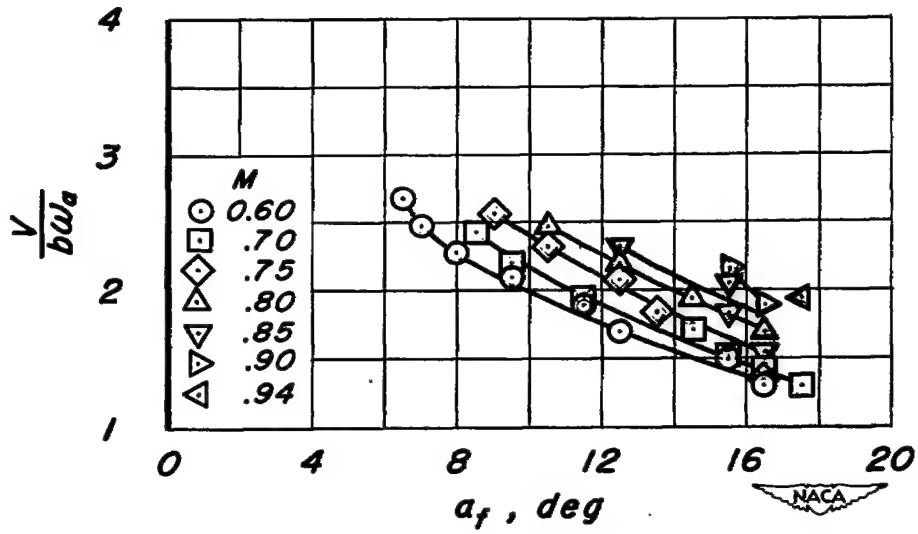

(b) Variation of $\frac{V}{b\omega_\alpha}$ with α_f.

Figure 14.- Effect of aspect ratio and Mach number on the stall flutter of wing 4AX.

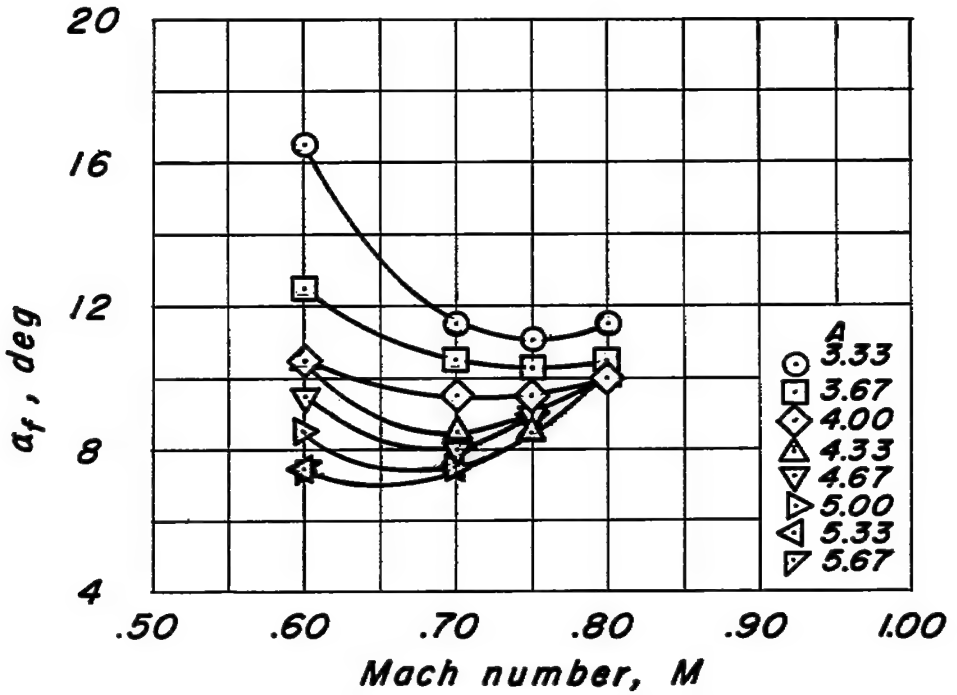

(a) Variation of α_f with Mach number.

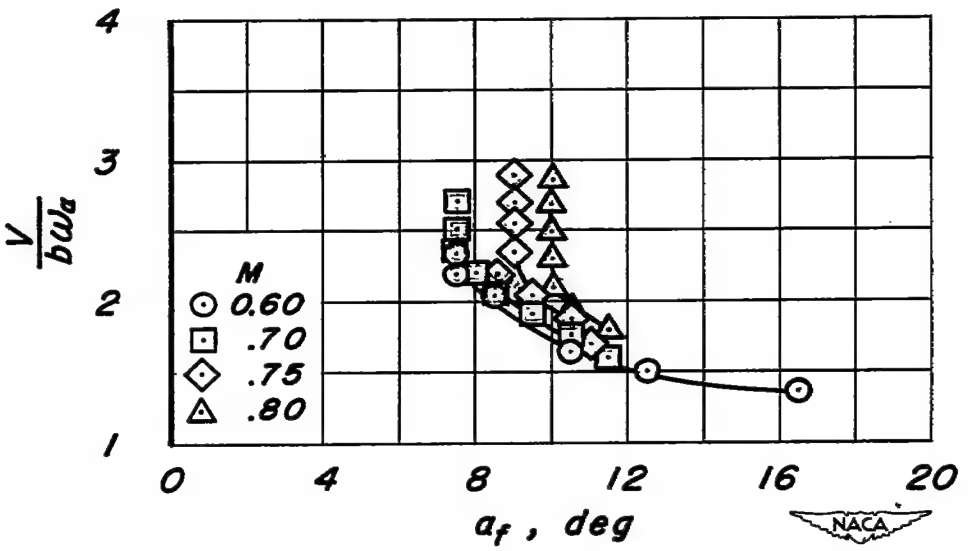

(b) Variation of $\frac{V}{b\omega_\alpha}$ with α_f.

Figure 15.- Effect of aspect ratio and Mach number on the stall flutter of wing 6AX.

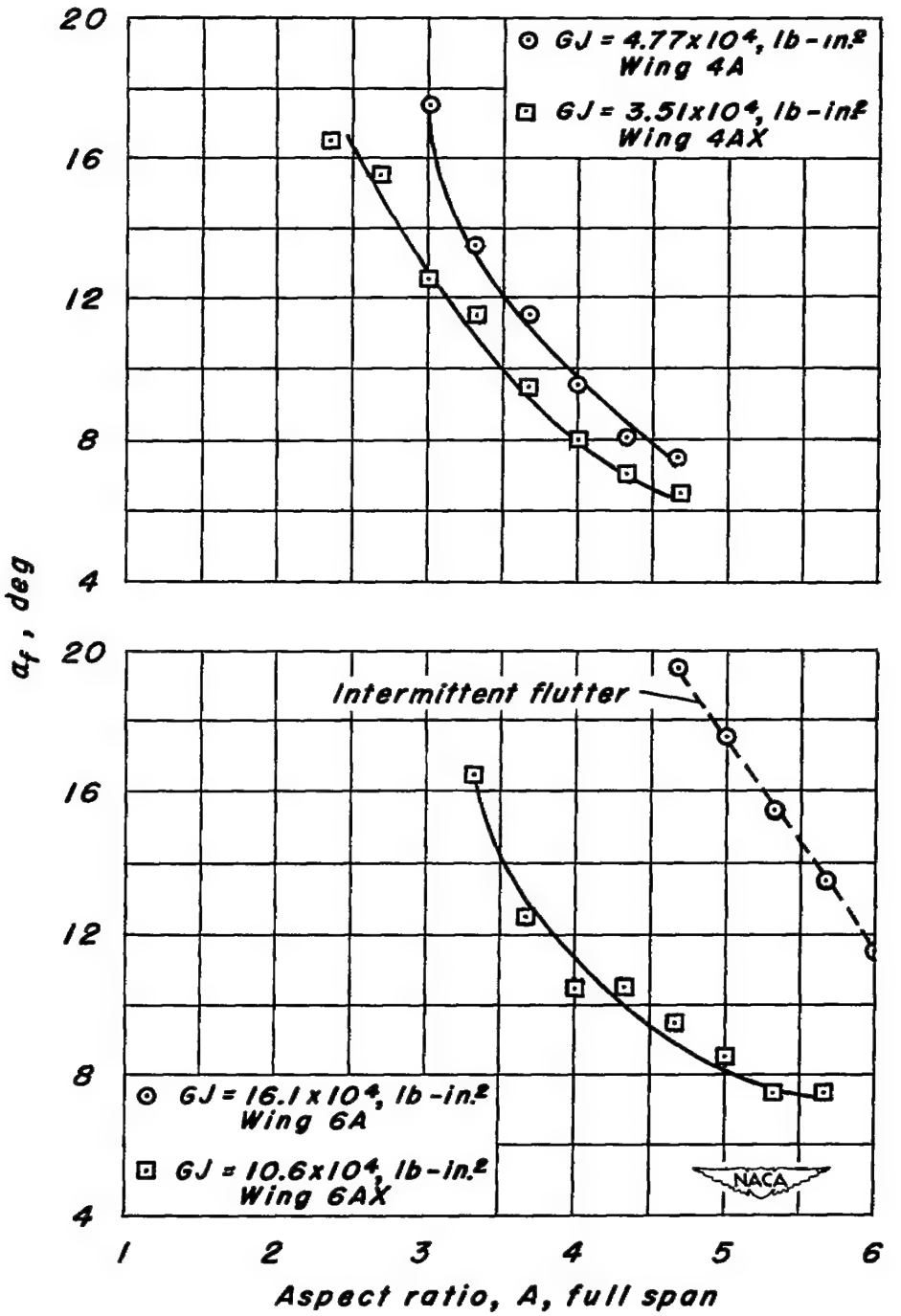

Figure 16.- Effect of a reduction in torsional stiffness on stall flutter at Mach number 0.60.

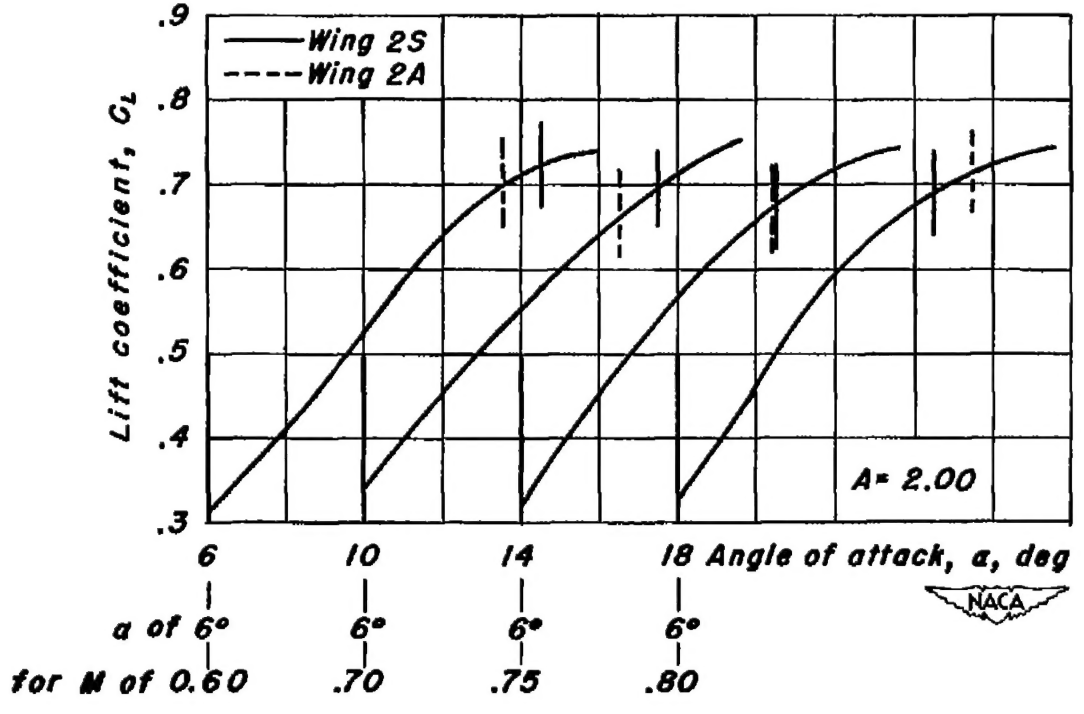

Figure 17.- Stall flutter of the 64A002 wings related to the static lift curves of a 63A002 wing.

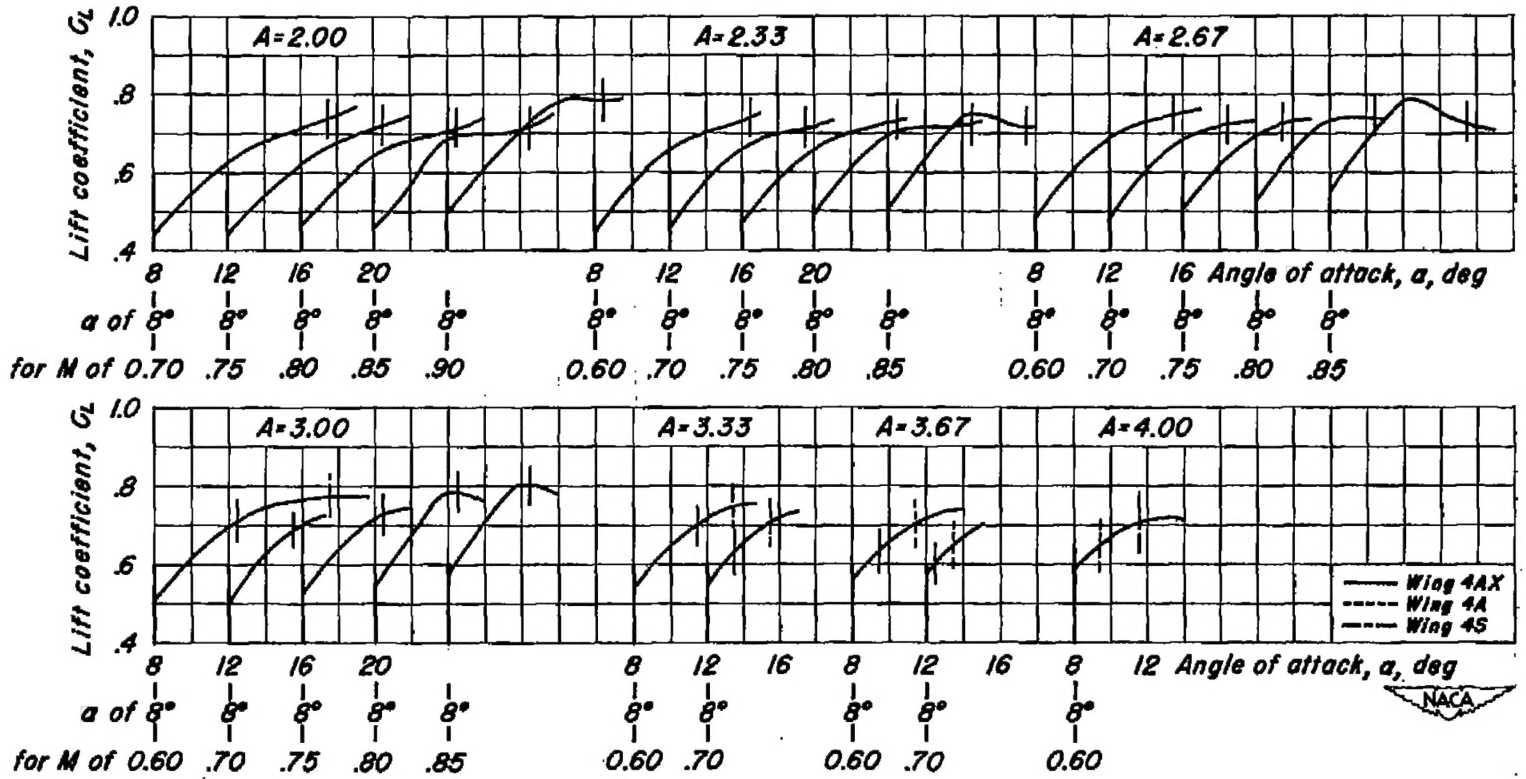

Figure 18.- Stall flutter of the 64A004 wings related to the static lift curves of a 63A004 wing.

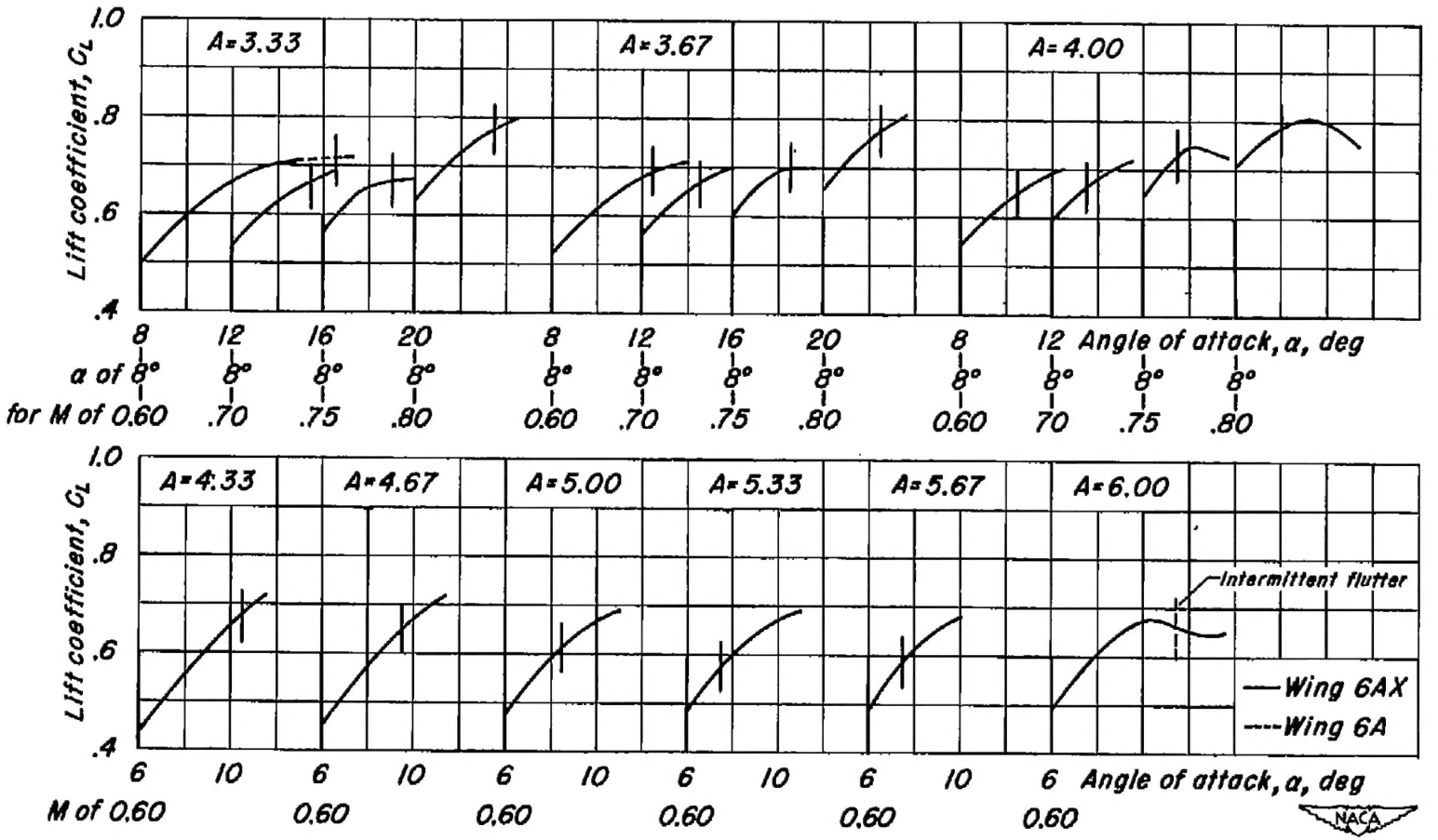

Figure 19.- Stall flutter of the 64A006 wings related to the static lift curves of a 63A006 wing.